NAVAL POSTGRADUATE SCHOOL

MONTEREY, CALIFORNIA

THESIS

UNDERWATER MULTIMODE DIRECTIONAL TRANSDUCER EVALUATION

by

Guilherme da Silva Sineiro

December 2003

Thesis Advisor: Thomas J. Hofler
Co-Advisor: Joseph A. Rice

Approved for public release; distribution is unlimited

THIS PAGE INTENTIONALLY LEFT BLANK

REPORT DOCUMENTATION PAGE		*Form Approved OMB No. 0704-0188*

Public reporting burden for this collection of information is estimated to average 1 hour per response, including the time for reviewing instruction, searching existing data sources, gathering and maintaining the data needed, and completing and reviewing the collection of information. Send comments regarding this burden estimate or any other aspect of this collection of information, including suggestions for reducing this burden, to Washington headquarters Services, Directorate for Information Operations and Reports, 1215 Jefferson Davis Highway, Suite 1204, Arlington, VA 22202-4302, and to the Office of Management and Budget, Paperwork Reduction Project (0704-0188) Washington DC 20503.

1. AGENCY USE ONLY	2. REPORT DATE December 2003	3. REPORT TYPE AND DATES COVERED Master's Thesis	
4. TITLE AND SUBTITLE: Underwater Multimode Directional Transducer Evaluation.		5. FUNDING NUMBERS	
6. AUTHOR(S) Guilherme da Silva Sineiro			
7. PERFORMING ORGANIZATION NAME(S) AND ADDRESS(ES) Naval Postgraduate School Monterey, CA 93943-5000		8. PERFORMING ORGANIZATION REPORT NUMBER	
9. SPONSORING /MONITORING AGENCY NAME(S) AND ADDRESS(ES) N/A		10. SPONSORING/MONITORING AGENCY REPORT NUMBER	

11. SUPPLEMENTARY NOTES The views expressed in this thesis are those of the author and do not reflect the official policy or position of the Department of Defense or the U.S. Government.

12a. DISTRIBUTION / AVAILABILITY STATEMENT Approved for public release; distribution is unlimited	12b. DISTRIBUTION CODE

13. ABSTRACT

An underwater piezoelectric directional transducer prototype, to be used in underwater acoustic networks, combines different vibration modes of a cylinder to synthesize desired beam patterns. Performance is evaluated in an anechoic water tank, with reference hydrophones and a signal analyzer capable of Fast Fourier Transform (FFT) data processing. An impulse technique is used for measuring impedance, admittance, Transmitted Voltage Response (TVR), Receiving Voltage Sensitivity (RVS), and horizontal and vertical beam patterns. In this technique, a single-cycle tone burst is emitted at a low frequency repetition rate and excites the driving transducer. The signal analyzer excludes the acoustic reverberations from the tank walls by adequate adjusting of the FFT sampling window. Additionally, for beam-pattern data acquisition, a computer simultaneously samples the azimuthal orientation of the prototype relative to a reference hydrophone and the corresponding frequency response, as the evaluated transducer continuously rotates. The FFT capability of the signal analyzer also supports intrinsic noise evaluation. The results show that the new transducer architecture is capable of producing directional beam patterns according to the present operational requirements by electronic control of the internal electrode applied voltage distribution.

14. SUBJECT TERMS Underwater Acoustics, Underwater Communication, Acoustic Modems, Directional Underwater Transducers, Piezoelectric Transducers, Acoustic Measurements, FFT Data Processing			15. NUMBER OF PAGES 69
			16. PRICE CODE
17. SECURITY CLASSIFICATION OF REPORT Unclassified	18. SECURITY CLASSIFICATION OF THIS PAGE Unclassified	19. SECURITY CLASSIFICATION OF ABSTRACT Unclassified	20. LIMITATION OF ABSTRACT UL

i

THIS PAGE INTENTIONALLY LEFT BLANK

UNDERWATER MULTIMODE DIRECTIONAL TRANSDUCER EVALUATION

Guilherme da Silva Sineiro
Lieutenant Commander, Brazilian Navy
B.S., Rio de Janeiro State University, 1984

Submitted in partial fulfillment of the
requirements for the degree of

MASTER OF SCIENCE IN ENGINEERING ACOUSTICS

from the

NAVAL POSTGRADUATE SCHOOL
December 2003

Author: Guilherme da Silva Sineiro

Approved by: Thomas J. Hofler
               Thesis Advisor

               Joseph A. Rice
               Co-Advisor

               Kevin B. Smith
               Chair, Engineering Acoustics Academic Committee

THIS PAGE INTENTIONALLY LEFT BLANK

ABSTRACT

An underwater piezoelectric directional transducer prototype, to be used in underwater acoustic networks, combines different vibration modes of a cylinder to synthesize desired beam patterns. Performance is evaluated in an anechoic water tank with reference hydrophones and a signal analyzer capable of Fast Fourier Transform (FFT) data processing. An impulse technique is used for measuring impedance, admittance, Transmitted Voltage Response (TVR), Receiving Voltage Sensitivity (RVS), and horizontal and vertical beam patterns. In this technique, a single-cycle tone burst is emitted at a low frequency repetition rate and excites the driving transducer. The signal analyzer excludes the acoustic reverberations from the tank walls by adequate adjusting of the FFT sampling window. Additionally, for beam-pattern data acquisition, a computer simultaneously samples the azimuthal orientation of the prototype relative to a reference hydrophone and the corresponding frequency response, as the evaluated transducer continuously rotates. The FFT capability of the signal analyzer also supports intrinsic noise evaluation. The results show that the new transducer architecture is capable of producing directional beam patterns according to the present operational requirements by electronic control of the internal electrode applied voltage distribution.

THIS PAGE INTENTIONALLY LEFT BLANK

TABLE OF CONTENTS

LIST OF FIGURES

THIS PAGE INTENTIONALLY LEFT BLANK

ACKNOWLEDGMENTS

As the thesis work comes to an end, I would like to express my deepest gratitude to the Brazilian Navy, for being entrusted with this mission.

To the faculty and staff of the Naval Postgraduate School, for their dedication, motivation and assistance in providing a worthwhile and rewarding educational experience.

To my international and American fellows, for extending my geographic boundaries of friendship and for sharing difficult and memorable moments of the academic life.

To my advisors, Professor Tom Hofler, for his wisdom, guidance and endless patience during the course and thesis work, and Joe Rice, for all enthusiasm, support and ability to provide constantly updated technical information.

To my brothers and relatives, for their constant encouragement and stimulus.

To my parents, for their love and unconditional belief in my achievements.

To my sons Nicholas and Brenno, for their brave withstanding of my long absence, and to my stepson Daniel, for his indulgence with my constant presence.

To my beloved wife Monica, for her dedication, endeavor, morale support, inspiration and joy.

Finally, to the One, for His enlightenment and protection along this journey.

THIS PAGE INTENTIONALLY LEFT BLANK

I. INTRODUCTION

A. PURPOSE OF THE WORK

The work described in the present thesis is intended to establish a procedure for analyzing directional transducers for future underwater wireless networks, as well as to carry out the performance evaluation of a multimode transducer prototype with respect to its main operational requirements. Measurement techniques were designed for application in the presence of physical limitations of the available facilities and the prototype development stage of the test unit.

B. DIRECTIONAL TRANSDUCER APPLICATIONS

The use of underwater acoustic networks as part of future sensor grids has been proposed as the basis of the undersea component of a distributed warfare architecture concept, also known as Forcenet (Clark, 2002). Underwater acoustic networks of autonomous sensors and vehicles, to be deployed in future naval operations, will extend naval net-centric operations into the undersea battlespace. In order to materialize this new operational capability, Rice (2000) proposed the Seaweb concept, which consists of a group of undersea wireless networks and associated gateway nodes that support through-water command and control (C^2), telemetry, and coordinated operations. The goal is to safely and reliably perform activities heavily dependent on data exchanged between network nodes, like environmental monitoring, surveillance, mine counter-measures and anti-submarine warfare (Figure 1).
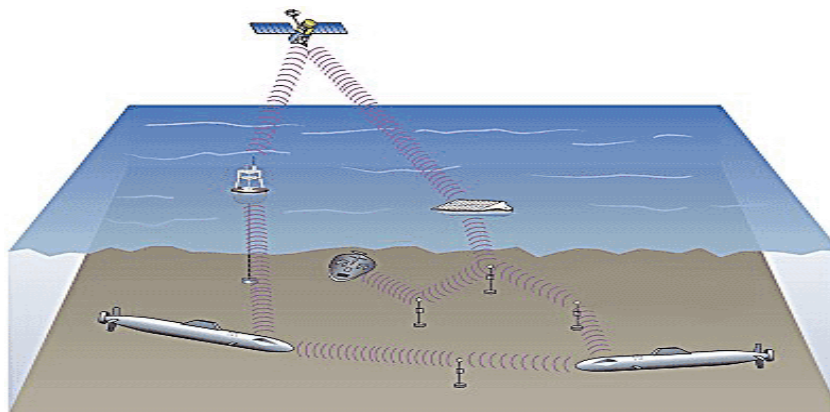
Figure 1.   Telesonar acoustic links interconnecting underwater nodes (Rice, 2003a).

The effectiveness of this architecture has already been proved in sea trials (Hartfield, 2003), but the standards for future undersea network operations demand increased transmission security through the use of higher acoustic frequencies, increased spectral bandwidth, spread-spectrum signaling and power control. In this context, directional electroacoustic transducers contribute to the improvement of the network performance, since they decrease battery-energy consumption, multi-user interference and interception by unauthorized listeners (Rice, 2003a). A theoretical computational model developed in the scope of the Seaweb project (Hansen, 2002) predicted the improved signal-to-noise ratio (SNR) with such transducers when their directivity index (DI) is compared to conventional, omni directional sources (Figure 2):
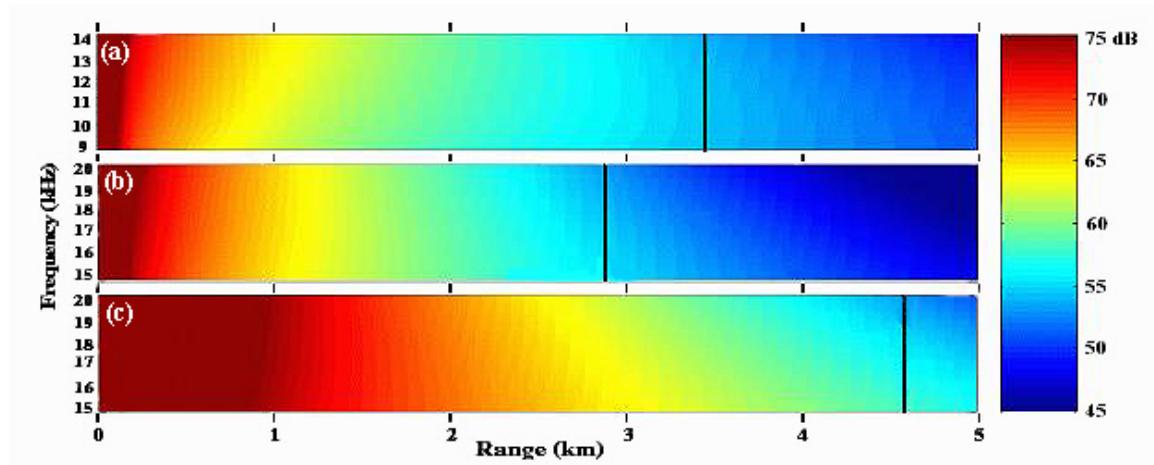
(a) DI = 0 dB (omni mode), 9-14 kHz bandwidth;
(b) DI = 0 dB (omni mode), 15-20 kHz bandwidth;
(c) DI = 9 dB, 15-20 kHz bandwidth;

Figure 2.   Transmitted SNR (color scale) and effective range (vertical bar) as functions of frequency (Hansen, 2002).

The theoretical predictions showed that a transducer transmitting at the conditions in Figure 2a suffers a reduction in its effective range when operating in higher frequency bands (Figure 2b). This attenuation is not only compensated by the increased directivity of the directional configuration in Figure 2c, but the effective range actually increases if compared with the original situation. These findings indicate that developing directional transducers is the natural step to be taken in the evolution of underwater wireless hardware.

2

C.   GENERAL CONFIGURATION

Several different piezoelectric transducer configurations have been proposed that are capable of attaining the desired directivity by electronically controlling the geometry of their beam patterns. Some of these alternatives are presented in Figure 3.
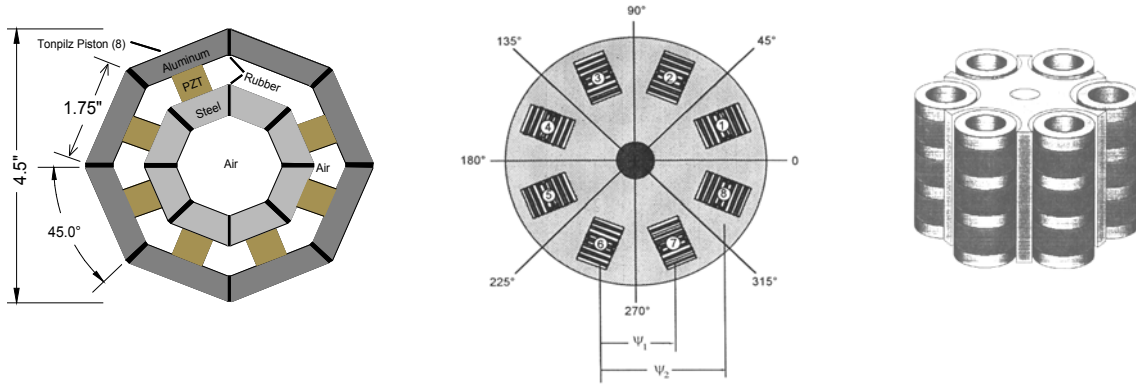
(a) Tonpilz ring (Image Acoustics, Inc.);
(b) Directional 1-3 piezocomposite (MSI);
(c) Baffled ring (BTech);
Figure 3.   Some proposed directional transducers (after Rice et al., 2003).

Alternative (a) was considered too heavy to be used in a floating device, while in proposition (b), the main obstacle was its high production cost. Finally, option (c) could not be adopted because of excessively large dimensions (Rice et al., 2003).

Figure 4 shows an early prototype and some aspects of the chosen design, presented by Butler, et al. (2000), as the multimode transducer.
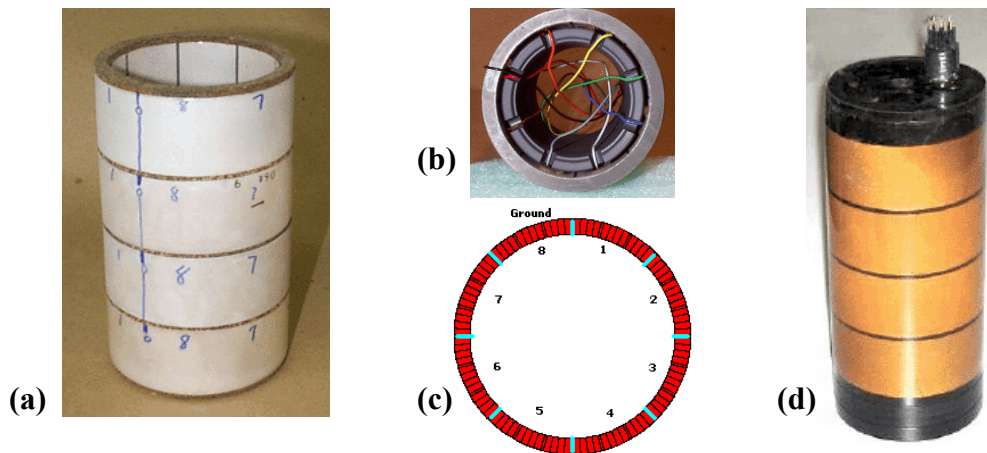
(a) Stack of four cylinders;   (b) Top view of internal wiring;
(c) Layout of the electrodes in a cylinder;   (d) Finished prototype;
Figure 4.   Early prototype of the multimode transducer (after Rice et al., 2003).

3

This last alternative is a stack of piezoelectric ceramic cylinders with electrodes on the internal and external surfaces (Figure 4a). In each cylinder, the external electrode is continuous and connected to ground while the internal electrode is formed by eight electrically independent sectors (Figures 4b and 4c). Although each piezoelectric ring is made of an integral ceramic material, in Figure 4c the separation between electrodes was emphasized in light blue for better visualization. In final form, a polyurethane layer covers the external wall of the stack and the upper and lower caps are made of rigid anodized aluminum (Figure 4d). The interior volume of the stack houses the electronic package necessary for sea operation, including transmitting power amplifiers, receiving preamplifiers, electronic compass and twist sensors. The transducer can be built with two, three or four cylinders connected in parallel, depending on the desired vertical beam pattern. Each cylinder has a height of 2 inches, an outer diameter of 4.25 inches and a wall thickness of 0.19 inches. The external diameter of the final polyurethane-potted transducer (Figure 4d) is 4.75 inches and the height depends on how many cylinders are used.

For directional transmission of acoustic signals, the piezoelectric material mechanically reacts to different voltages applied to the internal sectors, with the combination of extensional circumferential vibration modes of the cylinders, composing a beam pattern with axis in the steered direction. Directional reception is achieved through reciprocity, by selective amplification of the internal sectors oriented towards the desired azimuthal location.

Although the present transducer configuration still needs to receive internal electronic components in order to reach fully operational status, its lower weight, high mechanical strength and dimensional compatibility with current ocean-deployed devices characterize the architecture as the most appropriate alternative among all available options.

II.   MULTIMODE TRANSDUCER CHARACTERISTICS

A.   THEORETICAL BEAM PATTERN SYNTHESIS MODEL

1.   Cylinder Extensional Vibration Modes and Resonances

The main feature of the multimode transducer under evaluation is the ability to synthesize desired horizontal beam patterns by combining the three most fundamental extensional vibration modes of a cylindrical acoustic radiator. Neglecting axial stresses, the two-dimensional planar motion of a ring can be used to represent the dynamics of a short, thin-walled cylinder at resonance, efficiently loaded by the surrounding fluid. In this situation, the acoustic load on the cylinder causes most of the internal stress (Butler et al., 2000).
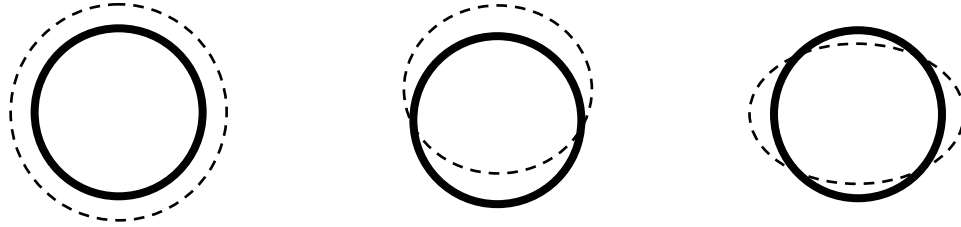
(a) Omni mode ($n = 0$);   (b) Dipole mode ($n = 1$);   (c) Quadrupole mode ($n = 2$);

Figure 5.   Two-dimensional planar motion representation of a cylindrical radiator.

The omni-directional or "breathing" mode shown in Figure 5a is the fundamental extensional mode that occurs when extensional waves travel a full wavelength distance around the ring circumference. In this mode, no vibrational nodes are formed since all circumferential locations have their extensional strains in phase, resulting in a purely radial displacement of the wall (Butler et al., 2000). The resonance frequency f_0 of this fundamental mode is given by

$$f_0 = \frac{c}{\pi D},$$

(1)

where c is the speed of sound for extensional waves in the ring wall and D is the mean diameter of the ring, defined as

5

$$D = \frac{d_o + d_i}{2}, \qquad (2)$$

in which d_o and d_i represent, respectively, the outer and inner diameters of the ring. According to Love (1944), once the fundamental frequency is known, the expression

$$f_n = f_0\sqrt{1+n^2} \qquad (3)$$

can be used to calculate the f_n frequencies of the subsequent n modes. Thus, for the dipole mode represented in Figure 5b, $n = 1$, and

$$f_1 = f_0\sqrt{1+1^2} = f_0\sqrt{2}. \qquad (4)$$

Figure 5c depicts the quadrupole mode, for which $n = 2$, yielding

$$f_2 = f_0\sqrt{1+2^2} = f_0\sqrt{5}. \qquad (5)$$

The three distinct, mode-related frequencies f_0, f_1 and f_2 have a direct impact in the behavior of the transmitting electrical response and receiving sensitivity of the prototype in multimode operation.

2.   Multimode Beam Synthesis

The extensional modes of interest for acoustic transduction are, in general, those presenting an even number of vibrational nodes along the circumference of the cylinder. In this case, each mode number n will generate $2n$ nodes, as seen in Figures 5a ($n = 0$, no nodes), 5b ($n = 1$, two nodes) and 5c ($n = 2$, four nodes). In practice, values of n higher than 2 (quadrupole) are not needed, since satisfactory directionality can be obtained by combining only the three most fundamental modes, which is exactly the case of the multimode transducer operational principle.

Butler et al. (2000) state that the total far-field complex acoustic pressure $\mathbf{p}(\theta)$ as a function of the azimuthal angle θ, resulting from a superposition of the three most fundamental extensional vibration modes of a cylinder, is defined by the normalized function

$$\frac{\mathbf{p}(\theta)}{\mathbf{p}(0)} = \frac{1 + \mathbf{A}\cos\theta + \mathbf{B}\cos 2\theta}{1 + \mathbf{A} + \mathbf{B}}, \tag{6}$$

where $\mathbf{p}(0)$ is the maximum far-field complex acoustic pressure of the major lobe, $\mathbf{A}$ is the normalized far-field acoustic pressure due to the dipole mode only, or

$$\mathbf{A} = \frac{\mathbf{p}_1(\theta)}{\mathbf{p}(0)}, \tag{7}$$

and $\mathbf{B}$ is the normalized far-field acoustic pressure due to the quadrupole mode only, which is given by

$$\mathbf{B} = \frac{\mathbf{p}_2(\theta)}{\mathbf{p}(0)}. \tag{8}$$

In expressions 6, 7 and 8, the complex, time-harmonic portion is represented by the factor

$$e^{j2\pi ft}, \tag{9}$$

where f is the frequency and t is the time. Since this factor is the same for the described pressures, all quantities become real after normalization, or

$$\frac{\mathbf{p}(\theta)}{\mathbf{p}(0)} = \frac{p(\theta)e^{j2\pi ft}}{p(0)e^{j2\pi ft}} = \frac{p(\theta)}{p(0)}, \tag{10}$$

$$\frac{\mathbf{p}_1(\theta)}{\mathbf{p}(0)} = \frac{p_1(\theta)e^{j2\pi ft}}{p(0)e^{j2\pi ft}} = \frac{p_1(\theta)}{p(0)} = A, \tag{11}$$

and

$$\frac{\mathbf{p}_2(\theta)}{\mathbf{p}(0)} = \frac{p_2(\theta)e^{j2\pi ft}}{p(0)e^{j2\pi ft}} = \frac{p_2(\theta)}{p(0)} = B. \tag{12}$$

The values assigned to A and B characterize the shape of the resulting beam pattern. Some of the more useful combinations are described in the following subtopics. It will be shown that, in practice, A and B are used as individual mode weights relative to the omni mode.

a.   *Cardioid*

This is a dual-mode beam pattern generated by the superposition of omni and dipole modes with same weights, as illustrated in Figure 6:

Omni Mode
Weight =1

Dipole Mode
Weight =1
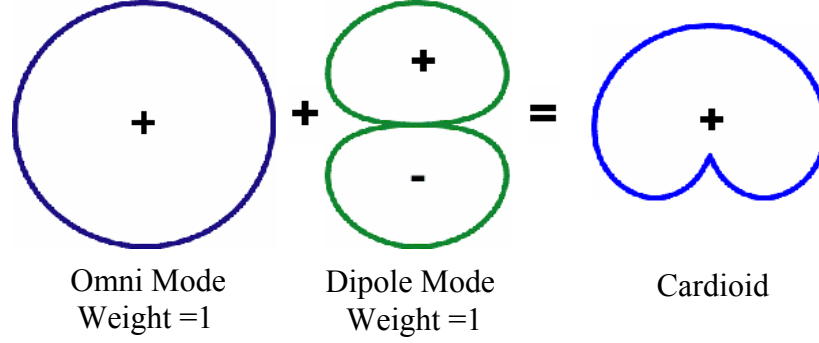
Cardioid

Figure 6.   Cardioid beam pattern shape (Butler et al., 2000).

For synthesis of this beam pattern, $A = 1$ and $B = 0$, resulting in the following normalized far-field pressure distribution:

$$\frac{p(\theta)}{p(0)} = \frac{1 + \cos\theta}{2}. \tag{13}$$

b.   *Trimode Cardioid ("Supercardioid")*

This cardioid is a trimode beam pattern obtained by the superposition of all three most fundamental extensional vibration modes (Figure 7).

Omni Mode
Weight = 1

Dipole Mode
Weight = 2

Quadrupole
Mode
Weight = 1
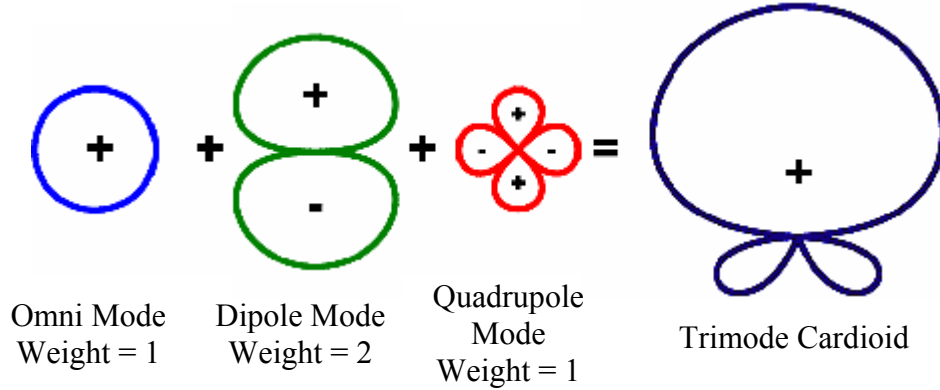
Trimode Cardioid

Figure 7.   Trimode cardioid beam pattern shape (after Butler et al., 2000).

The normalized far-field pressure distribution for $A = 2$ and $B = 1$ is

$$\frac{p(\theta)}{p(0)} = \frac{1 + 2\cos\theta + \cos 2\theta}{4}. \tag{14}$$

8

Figure 8 shows this trimode, which is actually a variation of the trimode cardioid beam pattern:
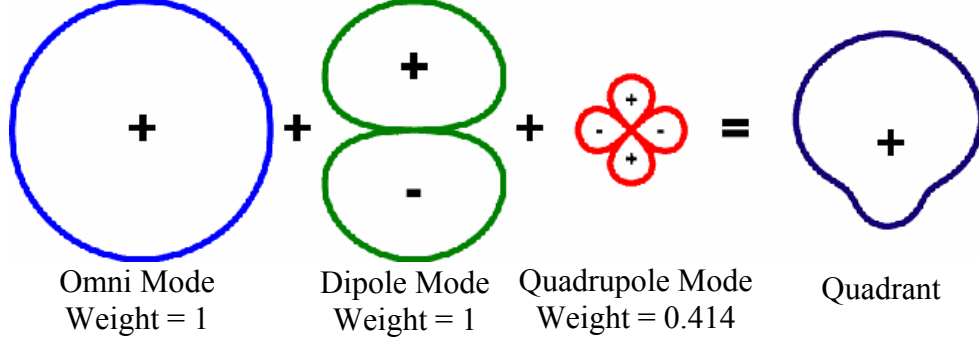
Figure 8.   Quadrant beam pattern shape (after Butler et al., 2000).

The values of A and B are 1 and 0.414, respectively, yielding

$$\frac{p(\theta)}{p(0)} = \frac{1 + \cos\theta + 0.414\cos 2\theta}{2.414}. \tag{15}$$

Butler et al. (2000) previously defined the quadrant beam pattern as a minimalist supercardiod because it minimizes the weight of the less-efficient higher modes in the beam pattern synthesis, improving overall efficiency.

The Seaweb architecture described in the introduction requires that the transducer operates in one of these multimode beam patterns or in omni mode, depending on specific applications. Different mode weight combinations can be further implemented as the operational requisites evolve.

B.   PROTOTYPE BEAM PATTERN SYNTHESIS

1.   Voltage Superposition Model

According to Butler and Butler (2003), to excite a given extensional vibration mode n in a piezoelectric ceramic cylinder, a circumferential electric field voltage distribution $\mathbf{V}_n(\theta)$, varying continuously with the azimuthal angle θ in the horizontal plane, has to be applied to the inner part of the cylinder, according to the following function:

$$\mathbf{V}_n(\theta) = \mathbf{V}_0 \cos n\theta. \tag{16}$$

In this function, $\mathbf{V}_0$ is the complex amplitude of the omni mode voltage distribution which, for a given instant in time, is constant in all radial directions and does not depend on θ. The connection between the values of $\mathbf{V}_n(\theta)$ and its corresponding normalized far-field complex acoustic pressure is provided by the expression

$$\frac{\mathbf{p}_n(\theta)}{\mathbf{p}(0)} = \mathbf{T}_n \mathbf{V}_n(\theta), \tag{17}$$

in which $\mathbf{p}_n(\theta)$ is the far-field complex acoustic pressure due to the n-th mode only, $\mathbf{p}(0)$ is the maximum far-field complex acoustic pressure and $\mathbf{T}_n$ is the complex amplitude of the Transmitted Voltage Response, or TVR, for the n-th mode (Rice et al., 2003). If the frequency dependency of the TVR is known for each mode, it is possible to compute the voltage distributions necessary to obtain specific beam patterns by superposition, since

$$A = \frac{\mathbf{p}_1(\theta)}{\mathbf{p}(0)} = \mathbf{T}_1 \mathbf{V}_1(\theta) \therefore \mathbf{V}_1(\theta) = \frac{A}{\mathbf{T}_1}, \tag{18}$$

and

$$B = \frac{\mathbf{p}_2(\theta)}{\mathbf{p}(0)} = \mathbf{T}_2 \mathbf{V}_2(\theta) \therefore \mathbf{V}_2(\theta) = \frac{B}{\mathbf{T}_2}. \tag{19}$$

This means that the same values of A and B previously defined for each beam pattern can be directly used to calculate the respective superposed voltages, to be applied in the inner segments. Additionally, as a major breakthrough of the multimode architecture, no complex voltage weighting or phase compensation is needed and purely real values are used for practical voltage distributions.

2.   Prototype Voltage Distribution

For a given mode n, a glance at the equations previously presented for the applied voltages reveals that the azimuthal angle θ is not limited to discrete values or to integer numbers. Consequently, in order to generate a perfectly smooth beam pattern, it would be necessary to apply a continuous voltage distribution along the internal electrode, which would demand a large number of segments. In practice, such an electrode is

10

expensive and difficult to build, but a set of equally spaced segmented electrodes produces similar results (Butler & Butler, 2003). The particular arrangement of eight segments, besides being easy and inexpensive to produce, is very useful because it yields symmetries that simplify the voltage distribution. An example of voltage distribution for synthesis of a trimode beam pattern is depicted in Figure 9 and the prototype beam pattern for four different frequencies is shown in Figure 10.

(a) Omni mode   (b) Dipole mode   (c) Quadrupole mode   (d) Trimode
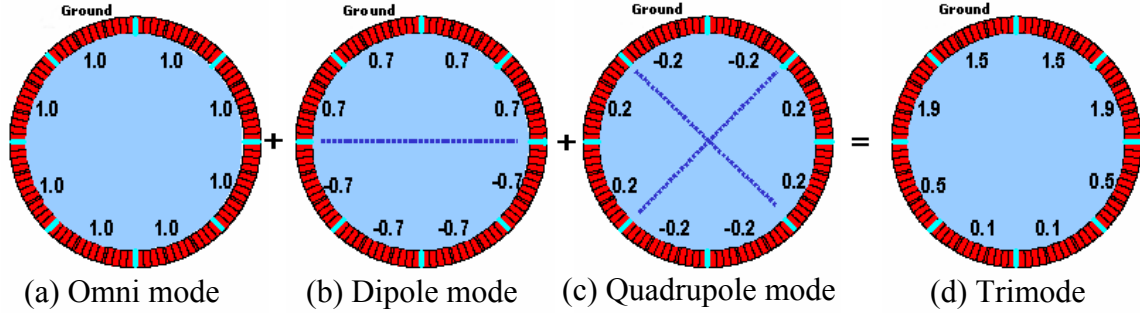
Figure 9.   Voltage distribution for synthesis of a trimode beam pattern (after Butler et al., 2000).

(a) Estimated Beam Pattern   (b) Measured beam pattern
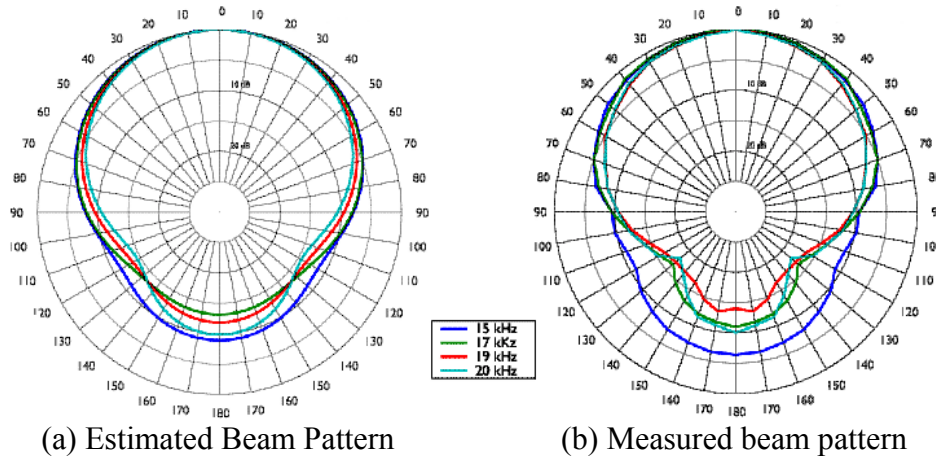
Figure 10.   Estimated and measured trimode beam patterns for four frequencies (after Butler et al., 2000).

According to Butler et al. (2000), preliminary test results of the prototype (Figure 10b) showed good agreement with the theoretical beam pattern values (Figure 10a), calculated by applying Finite Element techniques and the mathematical models previously discussed.

C. NOISE

The appendix of the present document contains a transcription of a detailed analysis of the noise generated by the multimode transducer when operating as a receiver, performed by Thomas Hofler (2003), Professor at the Naval Postgraduate School and Advisor of the present thesis work. The analysis was based on the results of the impedance measurements of the individual internal segments, as well as on the electronic circuit schematic, presented by the contractor (Acoustikos, Inc.) as the actual internal preamp, to be delivered inside the transducer packing.

According to the analysis, the noise generated by the piezoelectric ceramic alone is expected to be small and does not compromise the overall performance of the whole system. However, the preamp circuitry proposed by the contractor, in principle, may have a deleterious impact in the noise figures, depending on which prevailing underwater noise limit will be considered as acceptable.

Some important results from the analysis indicate that the estimated effective total equivalent input noise voltage density after signal summation is 10.2 nV/Hz$^{\frac{1}{2}}$ for the trimode operation, which is greater than the equivalent value when operating in omni mode (7.2 nV/Hz$^{\frac{1}{2}}$). Figure 11 depicts the estimated equivalent self noise pressure of the prototype in trimode operation, with original preamp circuitry, considering the measured values of Receiving Voltage Sensitivity (RVS). Two noise floor values (Wenz's minimum and Knudsen Sea State Zero) are also plotted for comparison.
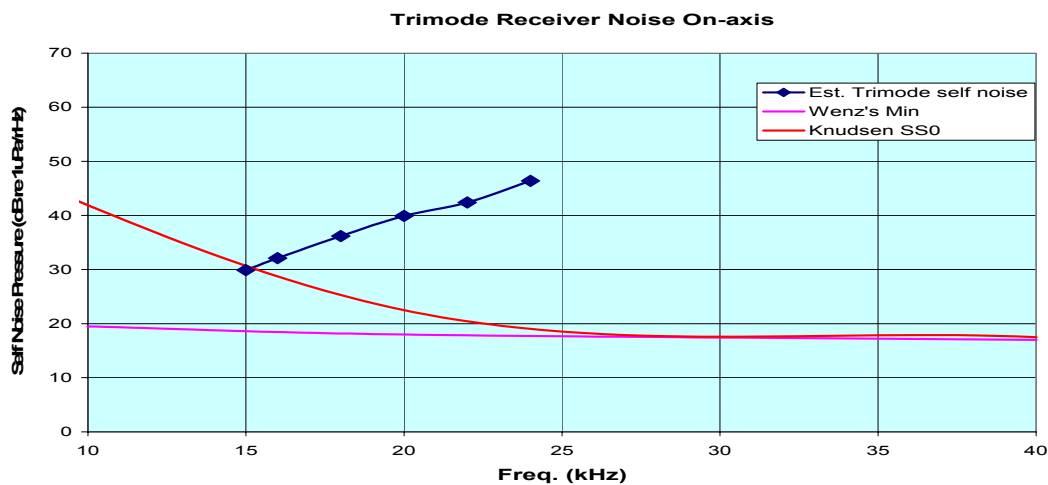
Figure 11.   Estimated trimode self noise pressure (after Hofler, 2003).

To mitigate the noise performance degradation by the preamp stage, Hofler suggests reviewing the values of some discrete elements of the original circuit, choosing only high quality circuit components and, alternatively, building a new preamp, based on discrete JFET transistors and utilizing tuning inductors. For this new circuit, the summed noise results could be as low as $3.6\,\text{nV/Hz}^{1/2}$ (without discrete JFET amplification). The effective total equivalent input noise voltage density would be $0.44\,\text{nV/Hz}^{1/2}$ for trimode operation, if the eight internal electrodes signals were to be conditioned and summed with noiseless amplifiers and circuitry.

THIS PAGE INTENTIONALLY LEFT BLANK

III.   PROTOTYPE PERFORMANCE EVALUATION

A.   OPERATIONAL REQUIREMENTS

Among the operational requirements described by Rice et al. (2003) for the multimode transducer, the following are of special interest:

- 5 kHz or more of bandwidth, starting at 15 kHz;

- Horizontal beam width of 60-90 degrees, equi-spaced radial beams;

- Vertical beam width of 70 degrees, fixed beam;

- Omnidirectional transmit and receive capability;

- Electronic transmit pointing;

- Electronic receive steering;

- Inexpensive in mass production;

- Compact size; and

- Efficient electroacoustic transduction.

It is worth mentioning that the efficiency quoted in the last requirement relates directly to the need of low power consumption. Thus, the electronic circuits to be placed in the interior of the operational transducer units will have to meet this requirement.

These constraints provided the basic specifications for designing the performance evaluation measurements described in this thesis work.

B.   TEST FACILITIES
1.   Anechoic Water Tank

The measurements of TVR, Receiving Voltage Sensitivity (RVS) and beam pattern were performed in an anechoic water tank in the basement of Building 232 (Spanagel Hall) at the Naval Postgraduate School. The layout and the approximated dimensions of the tank are listed in Figure 12. Both length and width were measured from the bottom of the absorbing panels and not from the concrete walls. The depth was measured from the water surface to the bottom panels.
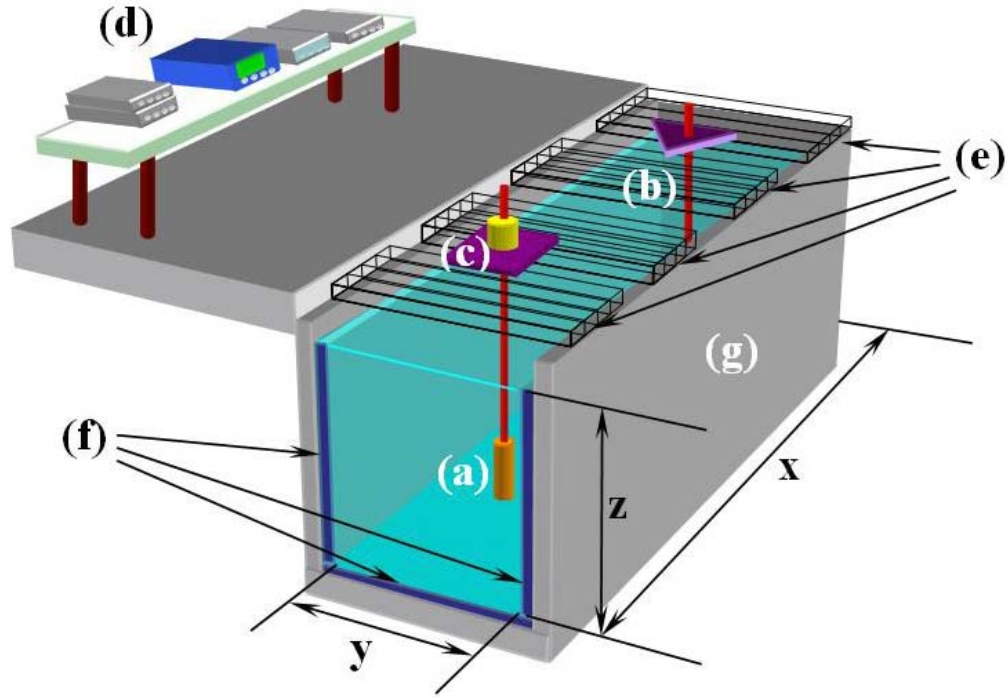
(a) Directional transducer prototype;
(b) Fixed reference hydrophone;
(c) Rotator with azimuthal angle reading;
(d) Electronic equipment bench;
(e) Adjustable floor grids;
(f) Sound-absorbing panels;
(g) Reinforced concrete structure;

x (m)	y (m)	z (m)
7.00	1.60	2.17

Figure 12.   Layout of the anechoic water tank.

Adjustable floor grids (Figure 12e) provided support for the transducers and flexibility to build different arrangements and to vary the distances between hydrophones. The grids also created a safe separation between the tank and the electronic measuring equipments placed on the lateral bench.   The sound-absorbing panels (Figure 12f), although not 100% effective, reduced undesired sound reflection inside the tank.

2.   **Equipment and Accessories**
In order to perform general measurements, data acquisition and transducer positioning, several instruments were used, as follows:

16

- Stanford Research Systems SR 785 two-channel dynamic signal analyzer;

- Stanford Research Systems SR 560 low noise preamplifier;

- Stanford Research Systems DS 345 synthetic function generator;

- Techron 5507 power amplifier;

- Dell Inspiron notebook;

- Step-up voltage transformer ($N = 7.56$);

- Current transformer (1 A = 1 V);

- Electrical motor-driven rotator with angle-proportional voltage output;

Additional accessories were also used to position the transducers at the correct distance and depth, like metallic supports and long cylindrical metallic rods.

All measurements were based on the Fast Fourier Transform (FFT) capability of the SR 785 signal analyzer, which provides instantaneous or averaged conversion of the measured signals from the time domain to the frequency domain. The SR 560 preamp, in turn, was chosen because of its very low noise characteristics, especially so when operating on batteries.

The Dell notebook used for beam pattern measurements consisted of a Pentium 4-based computer with 512 MB of memory. A pc-card with GP-IB interface sampled simultaneous angle and frequency response with triggering by the DS 345 function generator.

3. Transducers

The transducers used for the different tests were the International Transducer Corporation (ITC) model ITC-1032 (Figure 13a), as a projector and the Brüel & Kjær (B&K) hydrophone model 8103 (Figure 13b), as a receiver. The ITC transducer produces a beam pattern with good omni directional behavior (Figure 13c), while the B&K hydrophone has a flat response in the frequency band of interest (0 to 50 kHz), as show in Figure 13d.

17
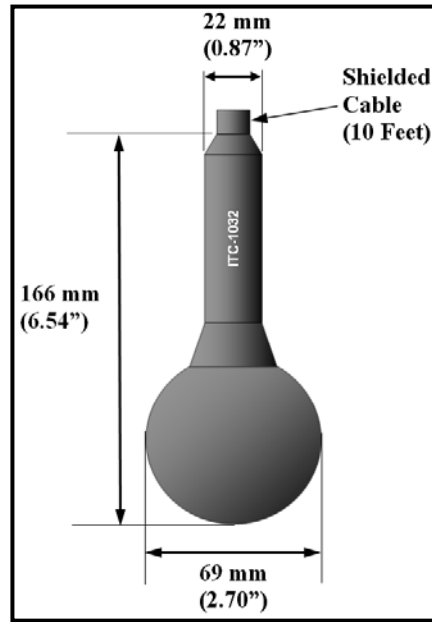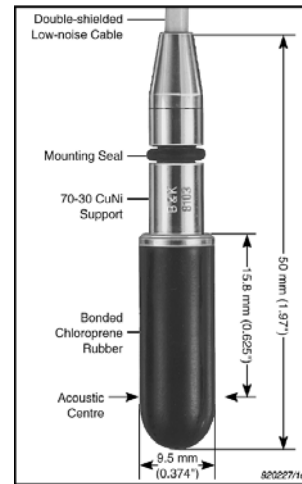
(a) ITC-1032 (driver)

(b) B&K 8103 (receiver)
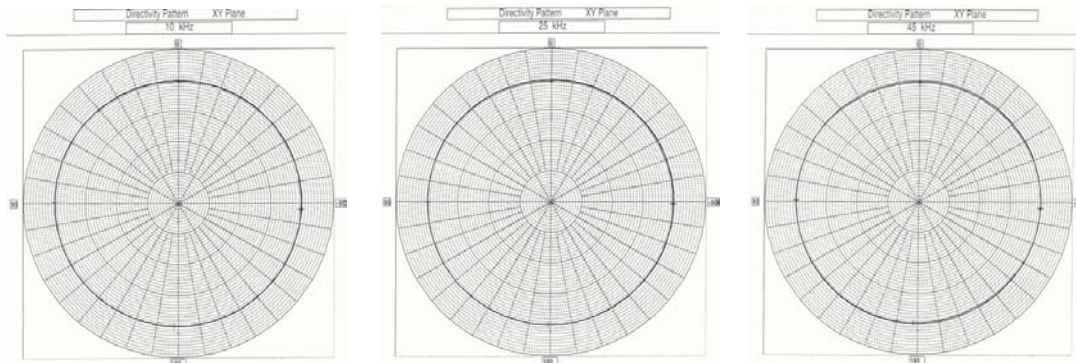
(c) ITC-1032 horizontal beam patterns at 10, 25 and 45 kHz
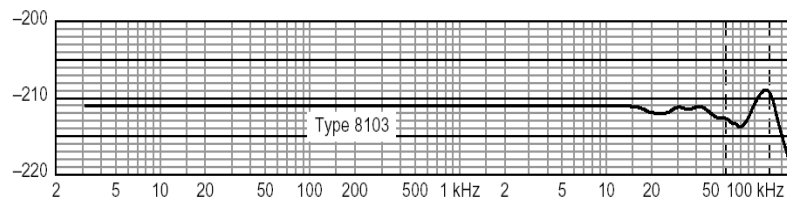
(d) Typical Receiving Voltage sensitivity of the B&K 8103 (dB re 1 V/μPa)

Figure 13.   Hydrophones used as acoustic drivers (after International Transducer Corporation, 2003) and receivers (after Brüel & Kjær, 2002).

18

C. INDIVIDUAL PARAMETER MEASUREMENT

All individual parameter measurements took advantage of either the swept sine wave signal processing or the FFT signal processing capabilities of the SR 785 signal analyzer. A particularly useful feature is the frequency response computation. This tool provides a frequency domain evaluation of the ratio between the FFT of the signal measured in channel 2 and the FFT of the signal measured in channel 1, also called reference channel.

1. Impedance and Admittance in Air and Water

The measurements of impedance and admittance of the multimode prototype were carried out in air and water with the help of a current transformer that converted the current passing through the prototype to a voltage, with a conversion ratio of 1 V/A (Figure 14).

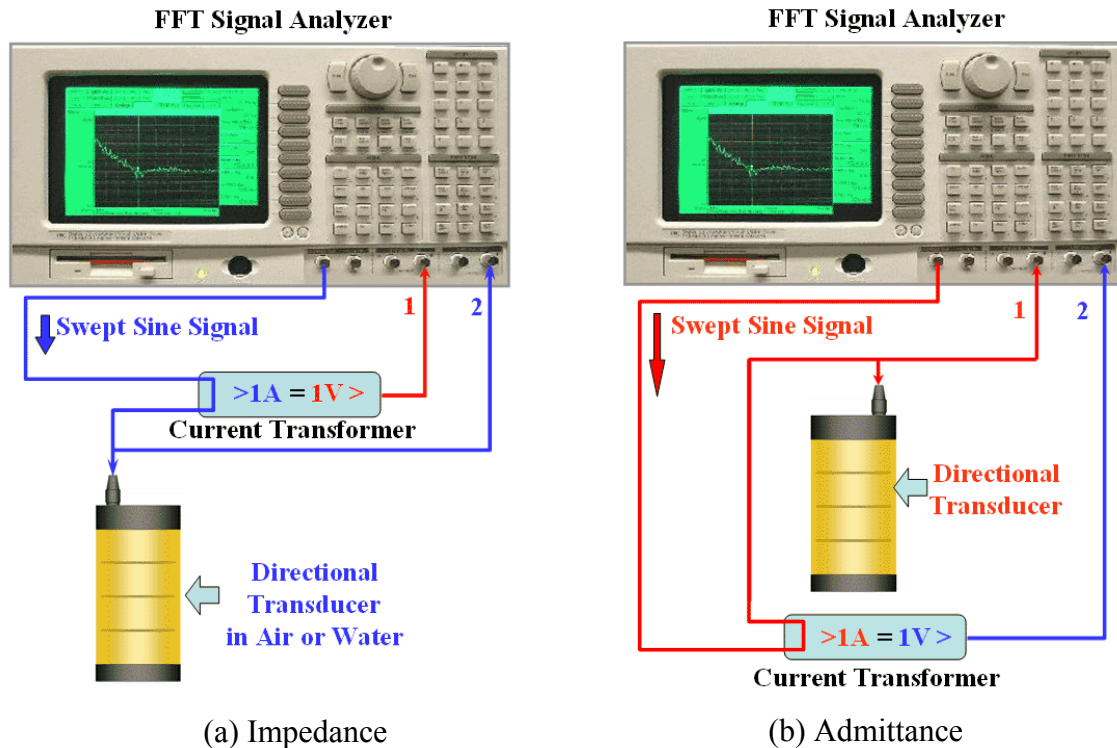(a) Impedance   (b) Admittance

Figure 14.   Layout of the impedance and admittance measurement setups.

As shown in Figure 14a, for impedance measurements, channel 1 (reference) measured the voltage proportional to the current passing through the directional

transducer, converted by the current transformer, while channel 2 received the swept sine voltage applied to the prototype. According to Ohm's Law, the ratio voltage/current, measured here as frequency response, yields the impedance values for the frequency interval of interest. For admittance measurements (Figure 14b), the voltage applied to the prototype was measured by channel 1 (reference) and the voltage proportional to the current was received by channel 2. In this situation, the frequency response will correspond to the current-to-voltage ratio, which is the same as the admittance of the prototype.

During impedance and admittance measurements in air, the directional transducer was positioned vertically on top of the equipment bench. A thick piece of foam was placed between the lower aluminum cap of the prototype and the bench to minimize vibration interference. For water measurements, the prototype was fixed by the upper cap and positioned vertically inside the water tank, at a depth of 1.08 m, which corresponds to half the total depth of the tank. The SR 785 signal analyzer generated a swept sine signal ranging from 5 to 25.6 kHz and the frequency response (FFT channel 2/FFT channel 1) was measured and recorded.

2. Impulse Measurements

In order to avoid the interference of reflected acoustic signals from the tank walls, an impulse technique was used for measurements requiring an underwater acoustic driving signal to excite the receivers. This technique consisted of exciting the driver hydrophone with a single-cycle, sinusoidal or square tone burst at a low repetition rate (usually 2 Hz). The trigger delay of the SR 785 signal analyzer was then visually adjusted so that the FFT time window contained only the direct acoustic signal arriving at the receiver hydrophones.

a. Transmitted Voltage Response

In this measurement, the multimode prototype is used as a source positioned inside the water tank, at 1 meter from the receiver, a Brüel & Kjær 8103 hydrophone (Figure 15). The DS 345 function generator produced a short sinusoidal or square tone burst that was amplified by the Techron 5507 power amplifier and injected in

the prototype. The same electrical signal was received by channel 1 (reference) of the SR 785 signal analyzer and compared with channel 2, which measured the output of the SR 560 preamp. The input of the preamp was connected to the B&K 8103 hydrophone.
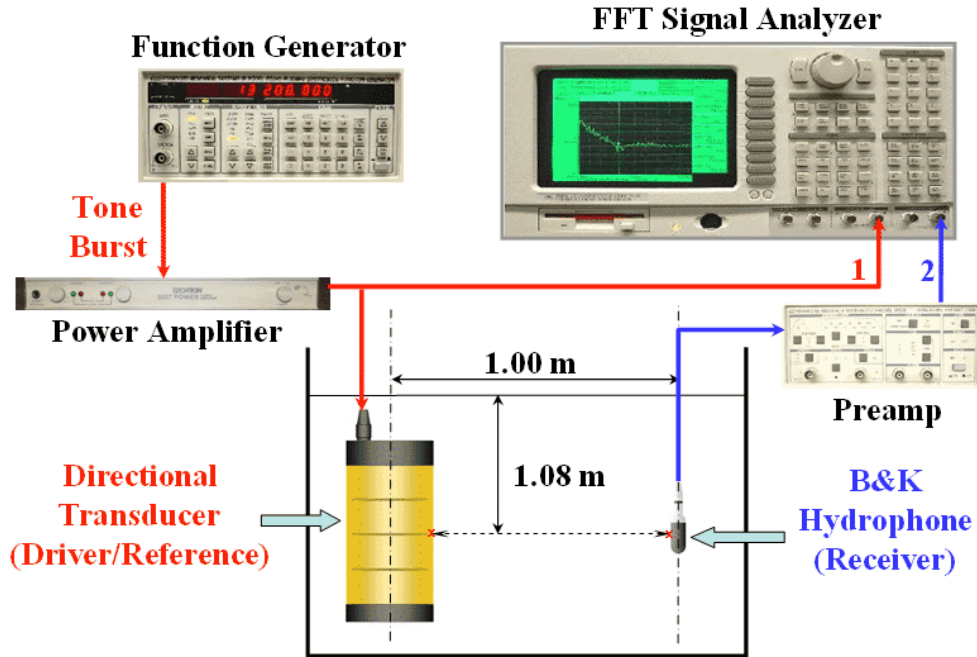
Figure 15.   Setup for TVR measurements.

It is shown in the picture that the acoustic centers of both transducers were aligned at a depth of 1.08 meters, which was considered to be half the total depth of the tank. The distance of 1 meter between transducers was chosen to produce the standard TVR results in dB re 1 μPa/V @ 1 m.

b.   Receiving Voltage Sensitivity

The working principle of the RVS measurement is to compare two electrical signals produced by two different transducers subjected to the same acoustic field. Although a collinear transducer arrangement is not the simplest possible configuration for a comparative measurement, it was used because of the different sizes and shapes of the transducers involved in this particular case. Figure 16 depicts the general arrangement of the transducers and electronic instruments.

Figure 16.   Setup for RVS measurements.

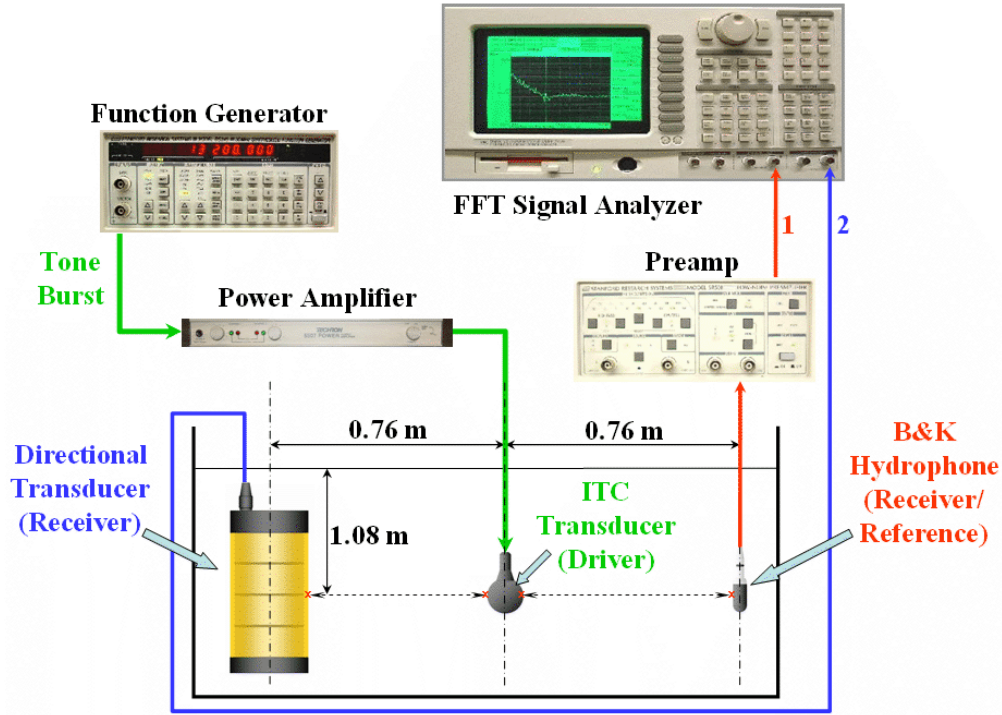The short tone burst generated by the DS 345 function generator was amplified by the Techron 5507 and applied to the ITC-1032 transducer, which acted as an acoustic projector. The B&K 8103 hydrophone was excited by the arriving acoustic signal and produced an electrical signal that was amplified by the SR 560 preamp and then injected in channel 1 (reference) of the SR 785 signal analyzer. Considering that the acoustic field produced by the ITC-1032 hydrophone is omni directional, the prototype received the direct acoustic excitation at the same time, producing a voltage that was applied to channel 2 of the signal analyzer. In this way, the resulting frequency response was referenced to the RVS of the prototype.

c.   *Horizontal Beam Pattern*

The same collinear arrangement and signal distribution described for RVS measurements was prepared for horizontal beam pattern evaluation. An electric rotator with azimuthal angle measuring capability was added to the layout, providing the multimode prototype with a constant rotation speed of 1 rpm. The DS 345 function generator produced a TTL sync pulse for each short tone burst generated, simultaneously

triggering the acquisition of instantaneous values of angle and frequency response by the voltmeter and the FFT analyzer and then transmitted to the Dell notebook, which was programmed to start and finish data acquisition at zero-degree reading. A layout of this arrangement is presented in Figure 17.

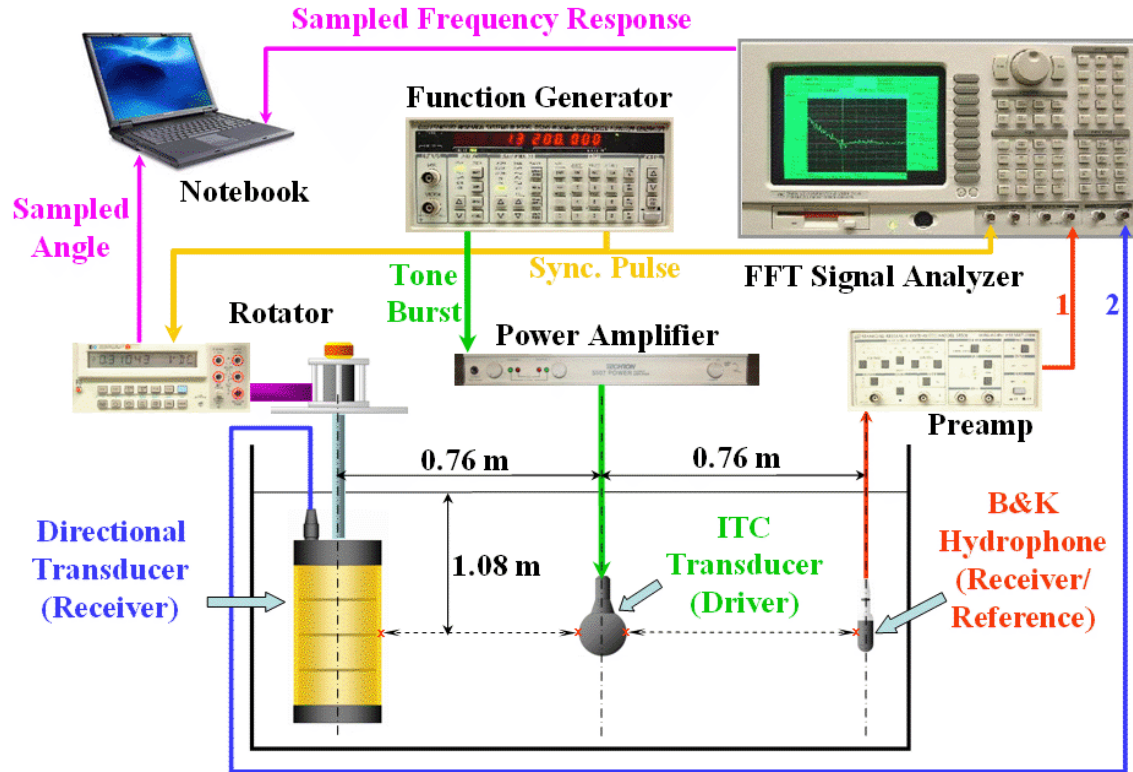Figure 17.   Setup for horizontal beam pattern measurements.

For frequency response sampling, the data acquisition program was designed to read the instantaneous value indicated by the screen cursor of the SR 785 signal analyzer, meaning that the transducer had to perform a full 360-degree turn for each frequency of interest in order to complete the corresponding horizontal beam pattern evaluation.

d. *Vertical Beam Pattern*

For receiving measurements on the vertical plane, the same arrangement used for receiving horizontal beam pattern was used, except for the prototype orientation. In this case, the central axis of the multimode transducer was positioned horizontally, as shown in Figure 18.
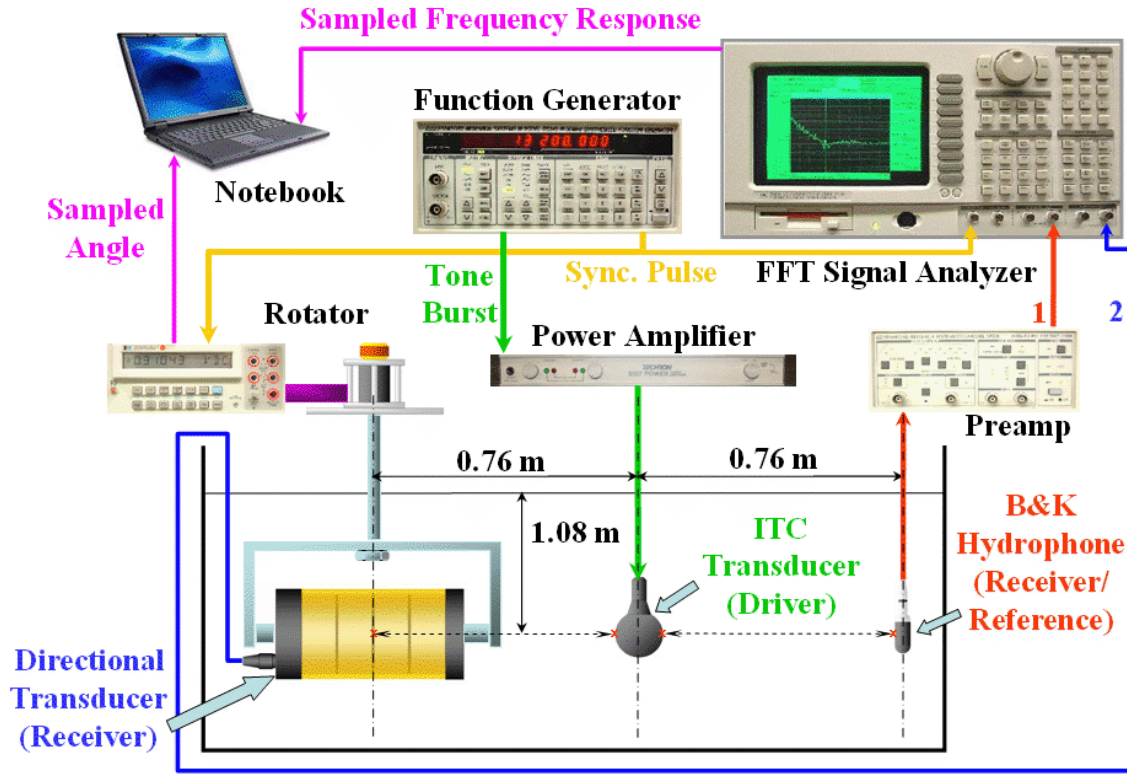
Figure 18.   Setup for vertical beam pattern measurement.

In this arrangement, the vertical beam pattern was evaluated for 3 different angles of the vertical plane of the main lobe with respect to the horizontal plane formed by the acoustic centers, as shown in Figure 19.

The angles corresponded to 0 degrees (Figure 19a), 45 degrees (Figure 19b) and 90 degrees (Figure 19c). For each main lobe angle, a full 360-degree turn was performed at a given tone burst frequency.
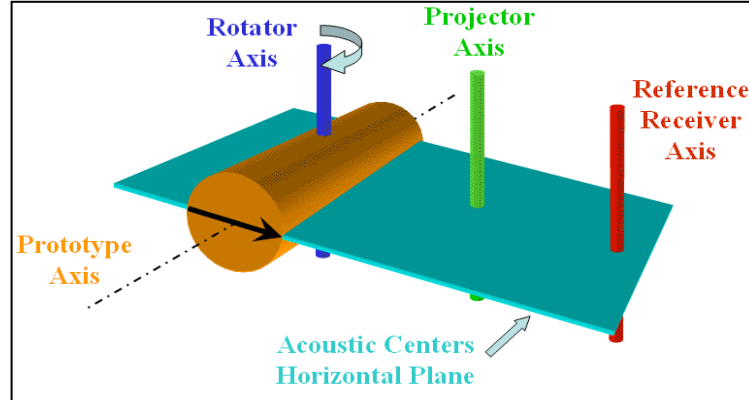
(a) Main lobe plane at 0 degrees, facing the projector.
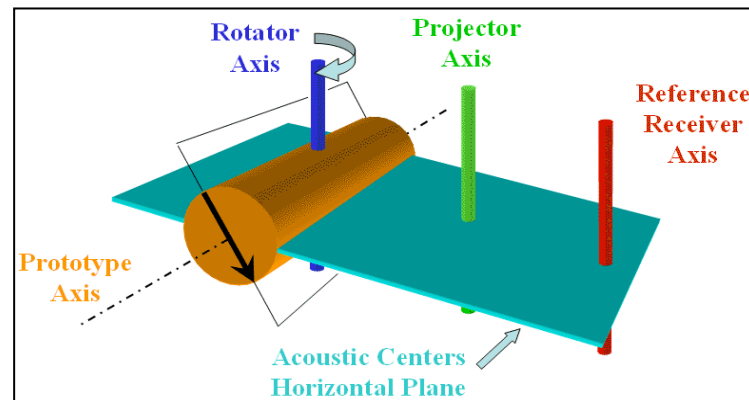
(b) Main lobe plane at 45 degrees, facing downwards.
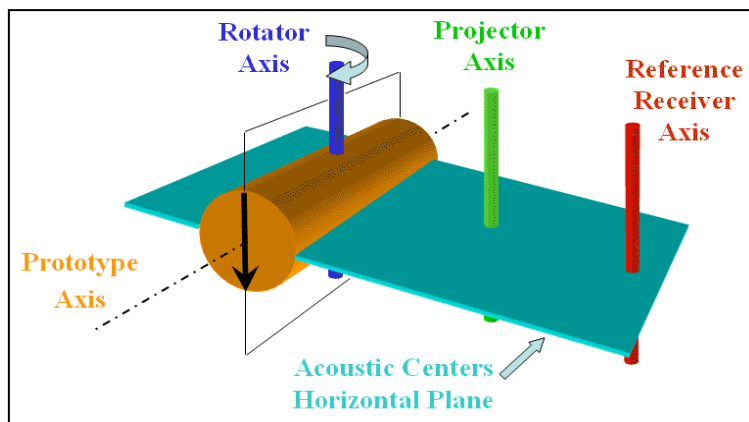
(c) Main lobe plane at 90 degrees, facing downwards.

Figure 19.   Position of the main lobe with respect to the horizontal plane of acoustic centers.

25

3. Noise

The electrical noise of the prototype was evaluated by directly measuring the power spectral density from the transducer output in air. The prototype was suspended by a cord and positioned as close as possible to the center of the anechoic chamber, located at the basement of Building 232 of the Naval Postgraduate School. The output of the transducer was connected to the SR 560 preamp, which, in turn, had its output connected to channel 2 of the SR 785 signal analyzer. The power spectral density values were acquired from channel 2 (Figure 20).
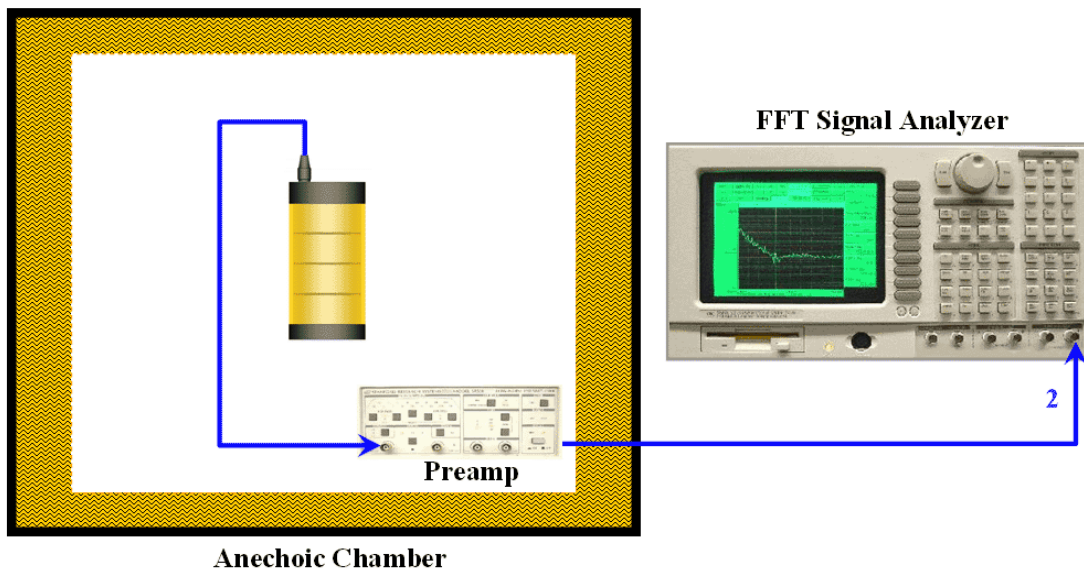
Figure 20.   Setup for noise measurements.

During the measurements, the preamp was disconnected from its AC power supply and operated on batteries to minimize the introduction of external electromagnetic noise from the AC grid. Adequate cable shielding and electrical contact was provided for all connectors. The measurements were made preferably at night, after a period of at least 24 hours from the time the prototype was put inside the anechoic compartment, in order to achieve an equilibrium temperature for the transducer with respect to the surrounding air.

IV.   ANALYSIS OF RESULTS

A.   IMPEDANCE AND ADMITTANCE

The following results correspond to a trimode configuration provided by a transformer connected to the inner electrodes of the transducer. The primary is attached to the measuring instruments, while the secondary provides the desired voltage distribution to the segments, which are connected in pairs (Figure 21).
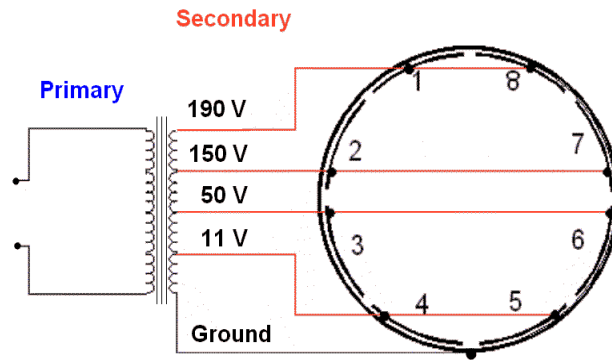
Figure 21.   Trimode transformer connections.
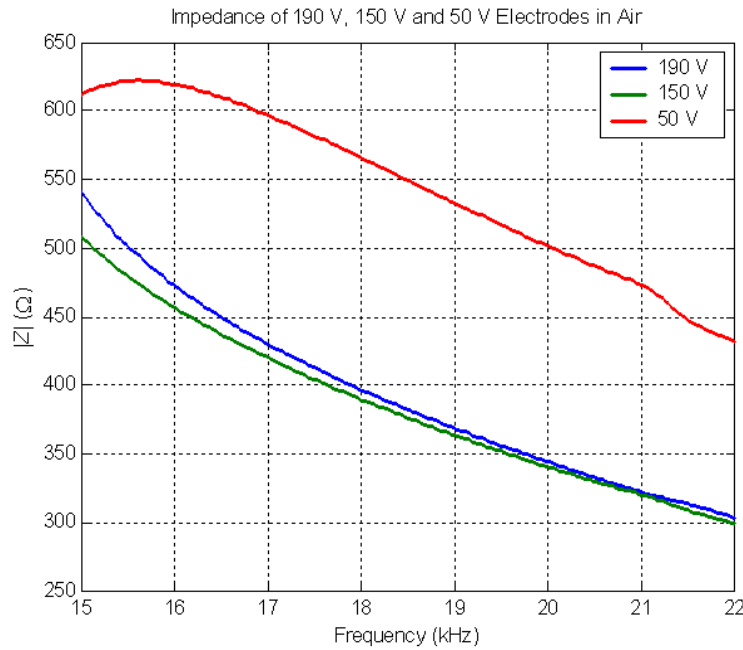
Figure 22.   Impedance of 190 V, 150 V and 50 V electrodes in air.
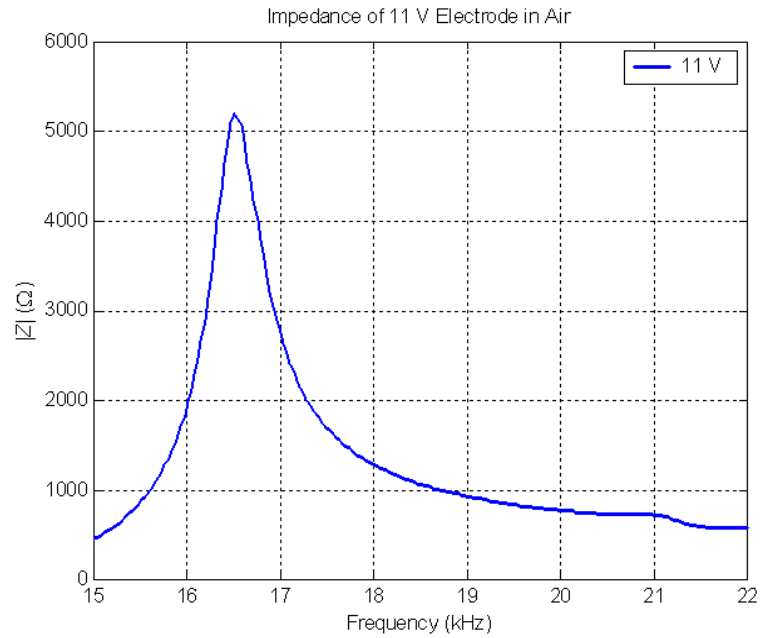
Figure 23.   Impedance of 11 V electrodes in air.
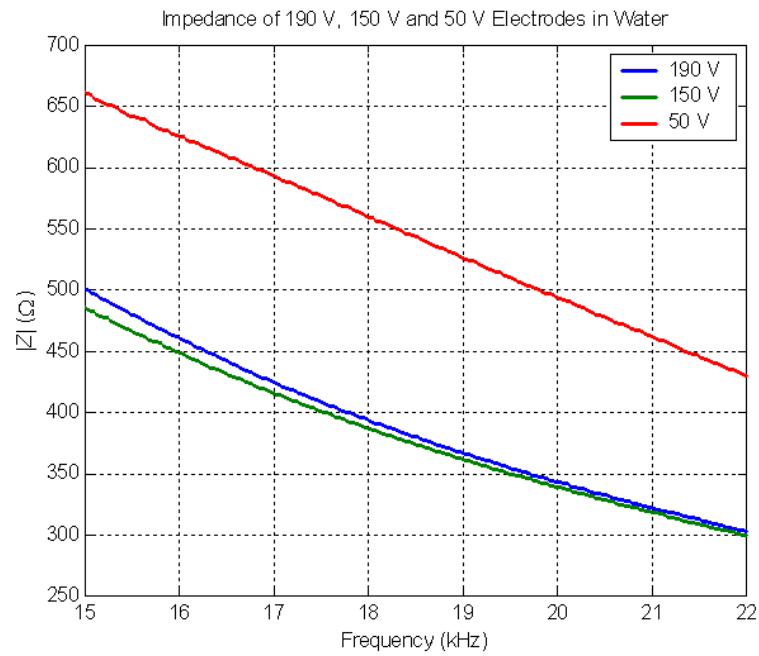
Figure 24.   Impedance of 190 V, 150 V and 50 V electrodes in water.
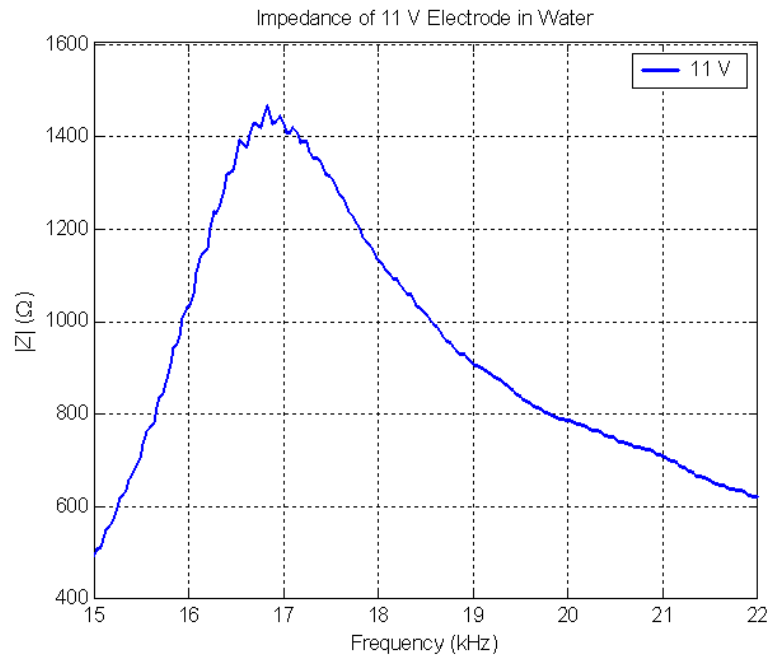
Figure 25.   Impedance of 11 V electrodes in water.

Considering the 190 V, 150 V and 50 V electrodes, the results show a consistent behavior for the impedance of a piezoelectric transducer. The 11 V electrodes presented a resonant peak between 16 and 18 kHz, probable due to interference from the 11 V tap impedance of the transformer.

29
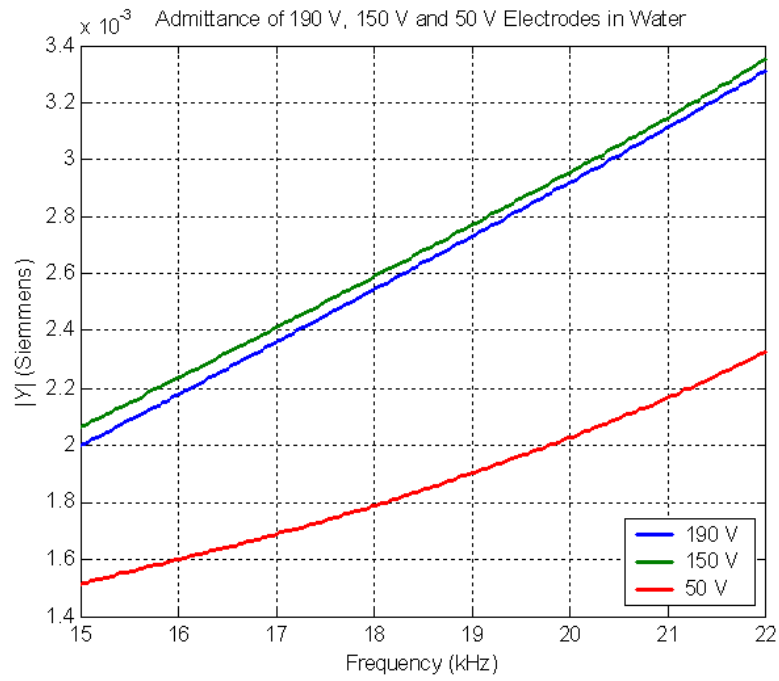
Figure 26.   Admittance of 190 V, 150 V and 50 V electrodes in water.
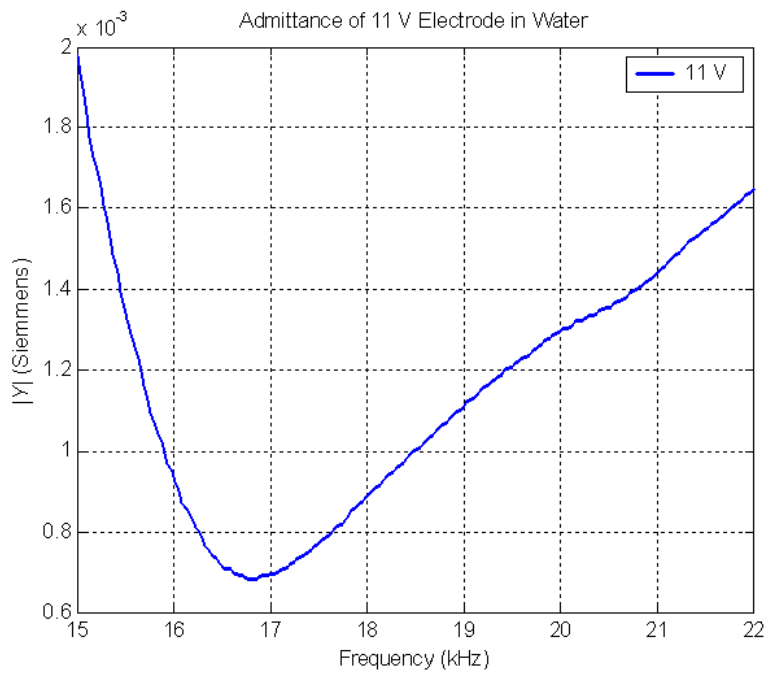
Figure 27.   Admittance of 11 V electrodes in water.

As in the case of impedance, the admittance results are compatible with a piezoelectric transducer, which behaves as a capacitive load. The 11 V pair of electrodes presents the same interaction with the transformer as in the impedance measurements.

For the omni mode measurements, all inner electrodes are connected in parallel, directly to the measuring instruments. The admittance of this mode in water is shown in Figure 28
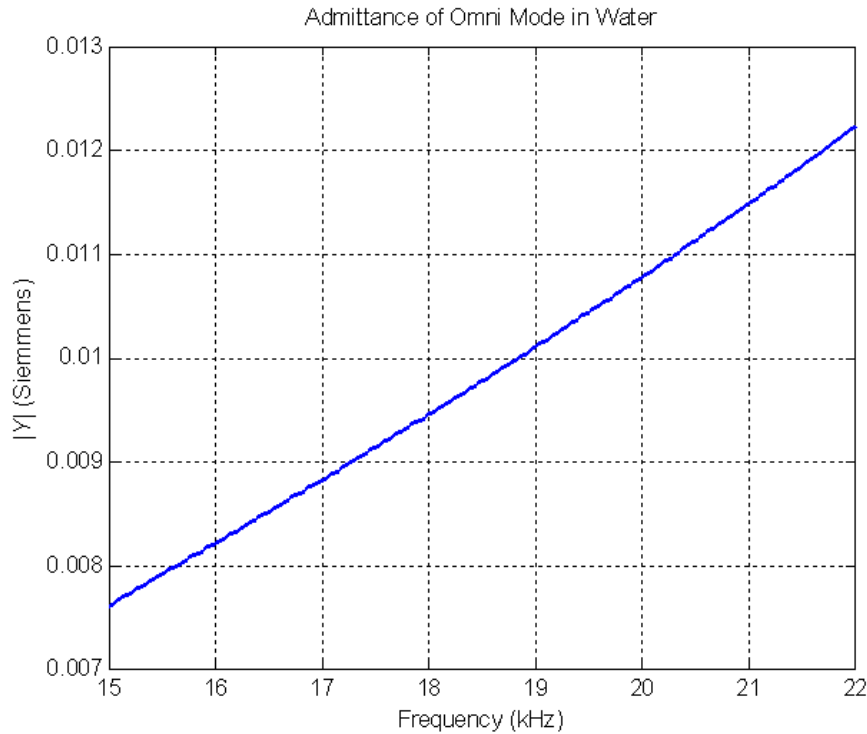
Figure 28.   Admittance of omni mode in water.

In this case, there is no inductive influence of the secondary of the transformer and the behavior of the prototype is of a purely capacitive load, as expected.

B. TRANSMITTING VOLTAGE RESPONSE
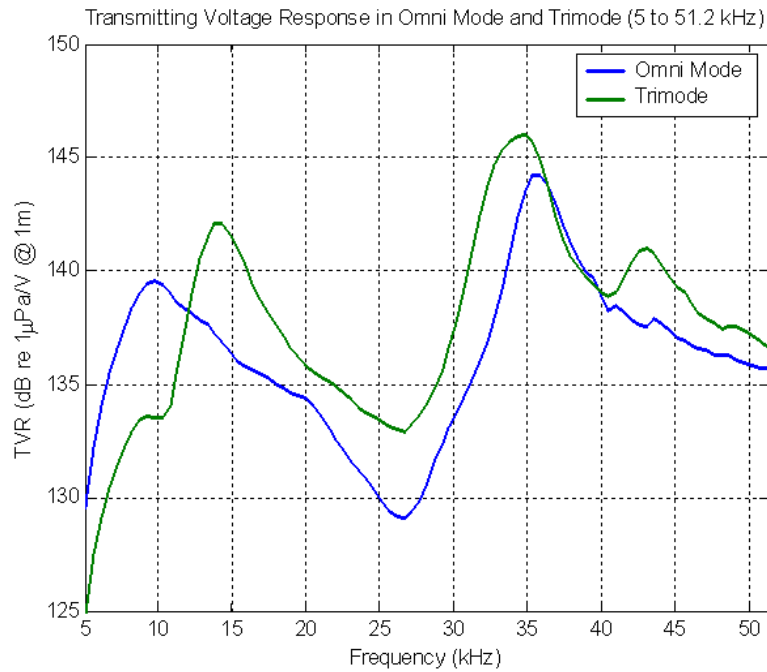
Figure 29.   TVR of omni mode and trimode (5 to 51.2 kHz).
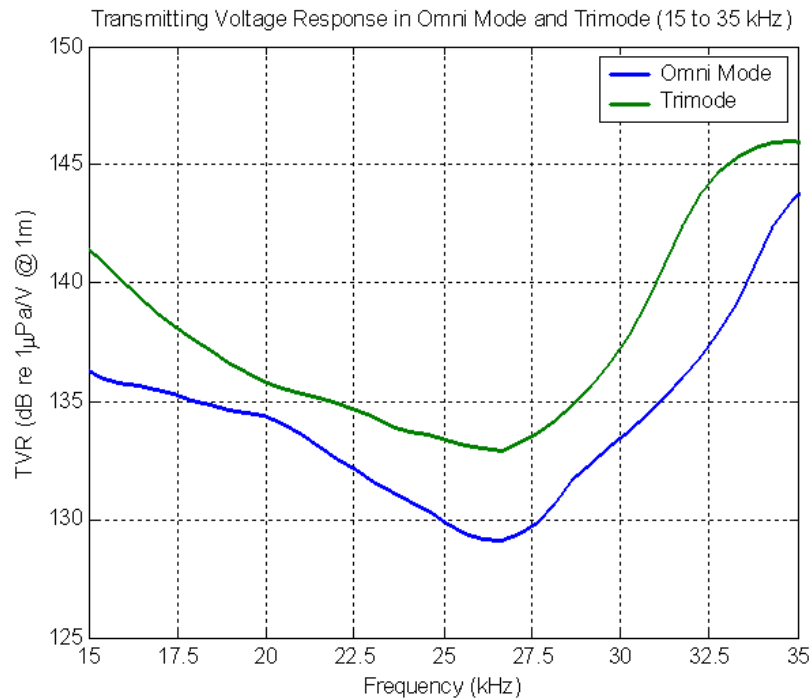
Figure 30.   TVR of omni mode and trimode (15 to 35 kHz).

The results of TVR measurements show two peaks for the omni mode operation (10 and 36 kHz) and two other peaks for the trimode operation (14 and 35 kHz), which correspond to the resonances of the dipole and quadrupole modes. Between these two frequencies, the minimum value for TVR occurs at around 26 kHz for both omni mode and trimode operations.

C.   RECEIVING VOLTAGE SENSITIVITY
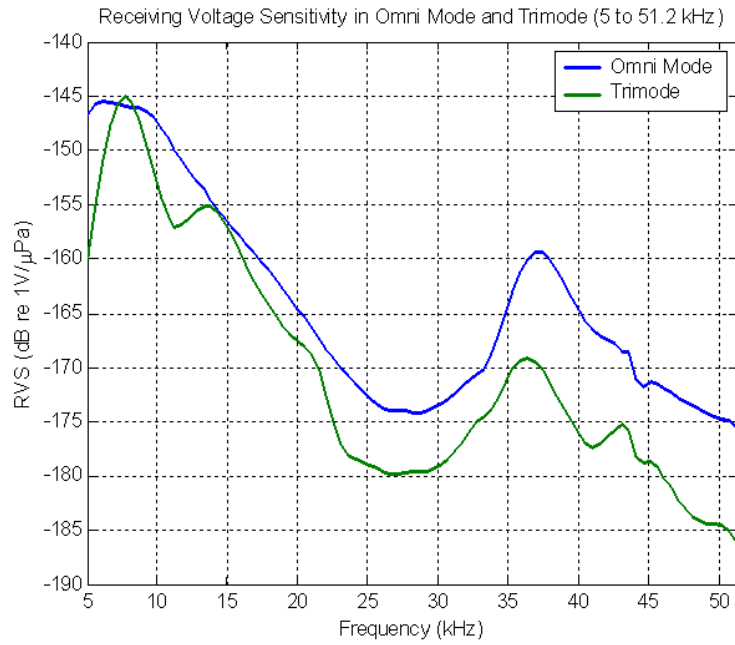
Figure 31.   RVS of omni mode and trimode (5 to 51.2 kHz).
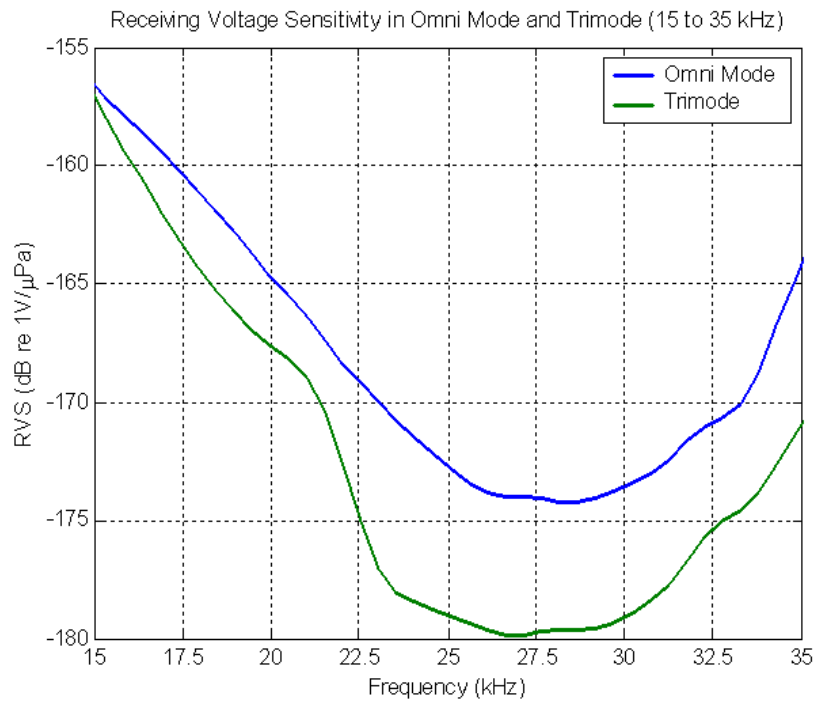
Figure 32.   RVS of omni mode and trimode (15 to 35 kHz).

34

The RVS behavior is very similar to that of TVR, in that two major peaks also occur. For the omni mode, these peaks are located at 6 and 37 kHz, and in the case of the trimode operation, they appear at 14 and 35 kHz. The influence of the dipole and quadrupole resonance frequencies is the main reason for this occurrence, and the overall response is consistent with the expected behavior.

D. HORIZONTAL BEAM PATTERN

Horizontal Beam Pattern in Trimode Operation (-5dB/division)
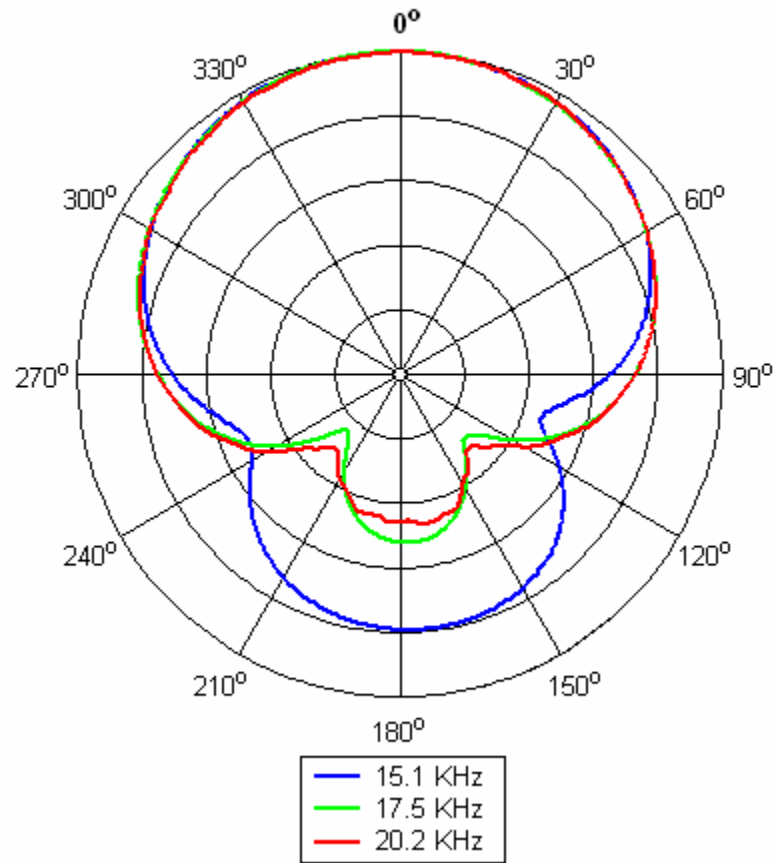
Figure 33.   Horizontal beam pattern in trimode operation (-5 dB per division).

The results show that the prototype is able to produce directional beam patterns in good agreement with theory. Additionally, it can be seen that the directionality in trimode operation increases with frequency, which is consistent with the proximity of omni mode resonance in lower frequencies.

E.   VERTICAL BEAM PATTERN

Vertical Beam Pattern in Trimode Operation (-5dB/division)
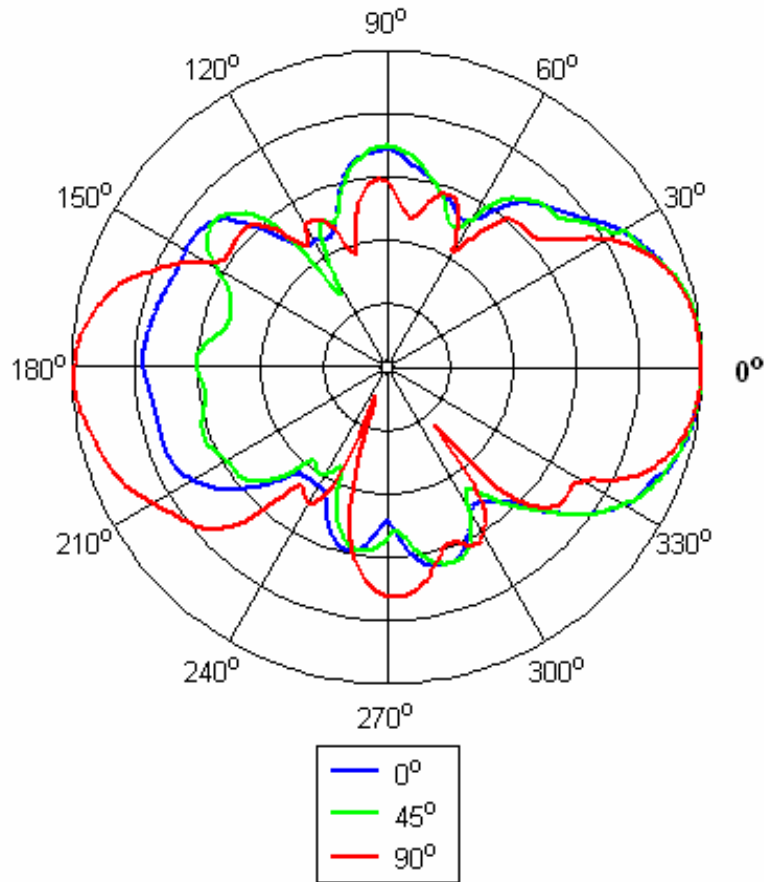
Figure 34.   Vertical beam pattern in trimode operation (-5dB per division).

The shape of the beam pattern is consistent with the expected vertical geometry. The vertical lobes at the center are probably due to coupling between the extensional and longitudinal vibration modes of the prototype.

THIS PAGE INTENTIONALLY LEFT BLANK

V. CONCLUSIONS

An impulse technique was employed to evaluate the Transmitting Voltage Response (TVR) and Receiving Voltage Sensitivity (RVS) of an underwater directional transducer prototype submerged in an anechoic water tank. The technique mitigated the undesirable sound reflections from the tank walls by limiting the transmitted pulse to a single-cycle tone burst with a low frequency repetition rate, and by adjusting the trigger delay of the signal analyzer, in order to include only the direct acoustic signal detected by the receiving hydrophone in the FFT window.

The same impulse technique was used to obtain the horizontal and vertical beam patterns of the prototype by adding a rotator to the directional transducer and a computer for data acquisition. For each tone burst, the azimuthal angle of the prototype with respect to the reference and the corresponding frequency response were simultaneously sampled and recorded for post-processing.

The multimode directional transducer prototype under evaluation employed a combination of the three most fundamental extensional vibration modes of a piezoelectric cylinder to synthesize steerable, directional beam patterns, as well as conventional, omni-directional beam patterns. According to the results, the prototype satisfied the current Seaweb operational requirements for bandwidth, horizontal and vertical directionalities, electronic beam steering and overall size.

THIS PAGE INTENTIONALLY LEFT BLANK

VI. SUGGESTIONS FOR FUTURE WORK

The beam pattern data acquisition system can be improved by allowing simultaneous recording of all values of frequency response for each azimuthal angle. A complete data acquisition system from B&K (Pulse System) is currently available to perform the same measurements. The equipment has an adjustable precision DC source, low-noise preamps and FFT processing capabilities, all integrated in one single console. Operation, data acquisition, mathematical processing and report generation are controlled by a Windows-based software, which is installed in a PC-compatible computer. After proper configuration, this equipment can increase overall measurement efficiency because of its integrated design, flexibility and simplicity of operation.

The noise performance of the preamplifier to be installed inside the transducer needs to be evaluated before pre-production phase, in order to ensure reliable operation of acoustic modems in low-noise ocean environments.

Both TVR and RVS of the prototype present a significant drop between 15 and 25 kHz. This fact, combined with the natural frequency-dependent sound absorption of salt water, can adversely affect the broadband operation performance of the transducer. Therefore, experiments at sea must be performed to evaluate the impact of attenuation of higher operational frequencies in that environment.

THIS PAGE INTENTIONALLY LEFT BLANK

APPENDIX

Modem Receiver Noise Analysis

Typical Receive Mode Circuit Operation

Below is the noise analysis of the original (Acoustikos) receiving electronics including PZT rings and PCB (printed circuit board) and op-amp. Note that the analysis is for one of 8 channels only. The 8 signals are summed down-stream on the PCB. The effect of the summation on the noise performance is discussed later.

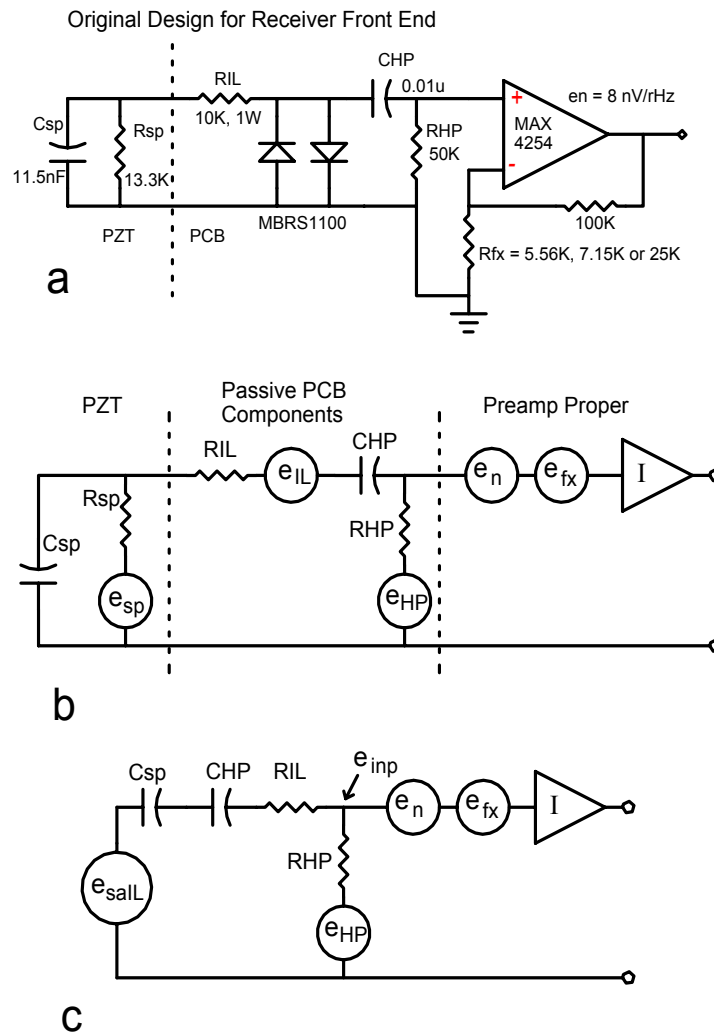**Figure 1. a) The original schematic. b) Equivalent noise circuit. Amplifier I represents an ideal noiseless amplifier. c) Simplified equivalent noise circuit.**

During acoustic transmission the 8 electrodes of the PZT are driven as 4 pairs of electrodes at voltages of 190 Vrms, 150 Vrms, 50 Vrms, and 11 Vrms. In receive mode the signals from each of the 8 electrodes are amplified by gains that are proportional to

43

the above transmit voltage values. If we normalize these voltages so that the maximum voltage of 190 Vrms becomes unity, we arrive at the following attenuations: 1.00, 0.79, 0.263, and 0.058. The 8 signals weighted in this manner are then summed in a summing amplifier.

The different gains are created by an analog multiplexer switching different values of R_{fx} in or out of the feedback loop of the op-amp circuit of Fig. 1 a). The dominant signals are the ones with the highest gain which correspond to $R_{fx} = 5.56k$. We will perform the noise analysis for this particular value.

Noise Theory

In Fig. 1 b) all of the significant thermal noise generators are indicated by the circular sources. These are all assumed to be Johnson noise sources where each one originates from a specific resistance with the exception of e_n, which is the equivalent input noise voltage of the op-amp. The effect of the input noise current of the FET input op-amp i_n, is assumed to be negligible and is ignored. These specific resistances are the following:

R_{sp} The effective parallel resistance of the PZT
R_{IL} The current limiting resistor
R_{HP} The high-pass filter resistor
R_{fx} The ground reference feedback resistor R_{fx} for the op-amp circuit

The protection diodes shown in Fig. 1 a) have an effective resistance also, but hopefully the resistance value is sufficiently large so that its noise is negligible.

Note, the resistance R_{sp} includes both the dissipative dielectric effects inherent in the PZT material as well as the increased resistance caused by the acoustic radiation from the PZT into the water, or vice versa. Because the acoustic radiation effect can be strong, the PZT impedance must be carefully measured in water. This measurement yields the parallel combination C_{sp} and R_{sp}.

The usual expression for the Johnson noise voltage spectral density of a resistor R is,

$$e = \sqrt{4kTR} \text{ Vrms/Hz}^{\frac{1}{2}} \tag{1}$$

The noise generated by the PZT resistance R_{sp}, is strongly attenuated by the reactance of C_{sp}. The correct expression for the resulting attenuated noise e_{sa}, is the Johnson noise filtered by an RC low-pass filter in the stop-band, or

$$e_{sa} = \sqrt{\frac{4kTR_{sp}}{1+\left(\omega R_{sp}C_{sp}\right)^2}} \cong \frac{\sqrt{4kTR_{sp}}}{\omega R_{sp}C_{sp}} \tag{2}$$

Also, once the attenuated noise e_{sa} is calculated, the impedance of the PZT can be approximated by the reactance C_{sp} only. Then it is possible to combine the two noise sources e_{sa} and e_{IL} into a single noise source in the following manner,

$$e_{saIL} = \sqrt{e_{sa}^2 + e_{IL}^2} , \tag{3}$$

44

assuming uncorrelated noise sources.

The noise entering the preamplifier stage is given by the noise value e_{inp}, which is a filtered combination of e_{saIL} and e_{HP}. If we define the total impedance of the element located between e_{saIL} and e_{HP} as Z_T, then

$$Z_T = \frac{1}{j\omega C_{sp}} + \frac{1}{j\omega C_{HP}} + R_{IL} + R_{HP} . \tag{4}$$

If we assume for the moment that the noise voltages represent the instantaneous voltages as a function of time, then the current flowing through Z_T is $I_n = (e_{saIL} - e_{HP})/Z_T$ and $e_{inp} = e_{HP} + I_n R_{HP}$. Combining the two equations we obtain,

$$e_{inp} = e_{saIL}\, R_{HP}/Z_T \ + \ e_{HP}(1 - R_{HP}/Z_T). \ (instantaneous) \tag{5}$$

If we now remember that the noise voltages are actually RMS averages and that two different sources will be uncorrelated, the correct noise voltage is,

$$e_{inp} = \sqrt{\left(e_{saIL}\left|\frac{R_{HP}}{Z_T}\right|\right)^2 + \left(e_{HP}\left|1 - \frac{R_{HP}}{Z_T}\right|\right)^2} \ . \tag{6}$$

Thus the total equivalent input noise voltage is,

$$e_T = \sqrt{e_{inp}^2 + e_n^2 + e_{fx}^2} \ . \tag{7}$$

Numerical Noise Results

Let's look at the values for the original circuit.

Component	Value	Units
R_{sp}	13.3	kOhm
R_{IL}	10.0	kOhm
R_{HP}	50.0	kOhm
R_{fx}	5.56	kOhm
C_{sp}	11.5	nF
C_{HP}	10.0	nF

Table 1.　　Passive component values.

Based on these values, we can calculate the equivalent and filtered noise values for a frequency of 17.5 kHz at room temperature, and arrive at an equivalent input noise voltage for the system given by e_T.

Noise V density	Value (nV/Hz$^{1/2}$)
e_{sp}	14.7
e_{IL}	12.7
e_{HP}	28.4
e_n	8.0
e_{fx}	9.5
e_{sa}	0.87
e_{saIL}	12.7
e_{inp}	11.6
e_T	17.0

Table 2   Equivalent noise voltage spectral densities for Fig. 1 a).

The final equivalent input noise voltage density of 17.0 nV/Hz$^{1/2}$ is not very good considering it is 6.5 dB above the noise floor of the op-amp.

Discussion of Noise Results

Let's scrutinize some of the noise voltage density values in the above table. While the value generated by the resistance inherent in the PZT and its transduction, e_{sp}, is rather large; the actual attenuated noise level from the PZT is e_{sa}, which is tiny. This is the fundamental noise floor of the system and while it is good that it is small, it is also too small to be conditioned perfectly on the PCB without a tuning inductor. Of course, it is possible to lower the PCB noise levels greatly, as we shall see.

The worst noise problem is the one generated by R_{IL} which is e_{IL}. It is particularly bad because both the level is high and because nearly all of it appears at the input to the preamp without attenuation. Why not lower the resistance value of R_{IL} by a factor of 10 or more? Because it is intended to limit the current passed to the protection diodes shown in Fig. 1 a) when the PZT is driven in transmit mode with more than 100 Vrms.

While the noise performance of the op-amp is good, it is not exceptional. However, those FET input op-amps with exceptional noise performance consume much more power from the battery supplies. One possible replacement is the LMV751 which has slightly higher power consumption and a noise floor of 6 nV/Hz$^{1/2}$ instead of 8 nV/Hz$^{1/2}$.

The final noise source that could be reduced is the one generated by the op-amp feedback resistor R_{fx}, which is switched between values ranging from 5.56 kOhms to

higher values by an analog switching device. This introduces $9.5\,\mathrm{nV/Hz^{1\!/2}}$ of noise voltage density and could be lowered considerably by lowering the resistance values of the feedback network. However, lowering the resistance values greatly will lead to errors caused by the on-resistance of the chosen analog switch (AD75019), which is about 200 Ohms. This can be mitigated by replacing the switch with a MAX308 which has an on-resistance of 100 Ohms and has a guaranteed matching of on-resistance between channels of 5 Ohms.

One final curiosity is the fact that the noise voltage density e_{inp} in Table 2 is 0.8 dB less than e_{saIL}. How is it possible that noise signal is lost at this point? The answer is that the R_{IL} and R_{HP} form a resistive voltage divider and $-1.6\,\mathrm{dB}$ of real receiver signal is lost too. This means that the true "effective" equivalent input noise voltage density is 1.6 dB higher than the value quoted in Table 2 for e_T. Compared to the signal strength that the PZT could have delivered to a high input impedance preamplifier, the corrected value is $e_T \rightarrow 20.4\,\mathrm{nV/Hz^{1\!/2}}$.

An Improved Circuit

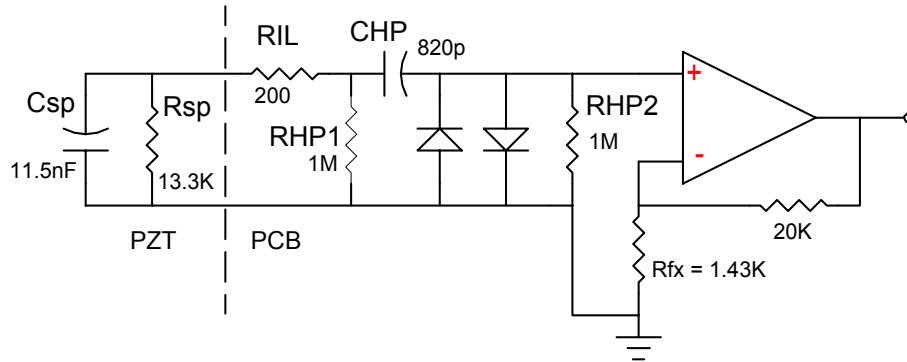An improved version of the circuit is shown below.

Fig. 2. A lower noise version of the circuit.

The noise analysis theory is roughly the same as before and is summarized in the following table where the original op-amp is retained. The effect of resistor RHP1 is ignored. Its presence is intended to prevent very large pyroelectric voltages from developing on the PZT.

Noise V density	Value (nV/Hz$^{1/2}$)
e_{sp}	14.7
e_{IL}	1.8
e_{HP2}	127.0
e_n	8.0
e_{fx}	4.8
e_{sa}	0.87
e_{saIL}	2.0
e_{inp}	2.5
e_T	9.7

Table 3.   Equivalent noise voltage spectral densities for Fig. 2.

Now the equivalent input noise voltage density is 9.7 nV/Hz$^{1/2}$ which is a –6.5 dB reduction compared to the original circuit. If an op-amp with 6 nV/Hz$^{1/2}$ were to be used in conjunction with a minimum R_{fx} = 500 Ohms, the noise level would be 7.1 nV/Hz$^{1/2}$ for a –9.2 dB noise reduction compared to the original.

An interesting detail about the circuit of Fig. 2 is that the capacitor C_{HP} serves a dual purpose of being both a high-pass filter component and the primary current limiting component that protects the protection diodes. The typical impedance of C_{HP} during transmit operation is roughly 10 kOhms. The resistor R_{IL} serves only as a second line of protection against PZT voltage surges having a very fast rise time. The diodes should be able to tolerate a few amperes of current on the 10 µs time scale.

Further improvements in the noise performance could be obtained with discrete JFET amplification. These could be integrated into the existing op-amp preamplifier circuit, or could be added as an entirely separate preamplification stage. A common JFET such as the 2N5484 (or MMBF5484 in surface mount) is capable of 3.0 nV/Hz$^{1/2}$ suggesting that, with effort, an e_T in the neighborhood of 4.0 nV/Hz$^{1/2}$ is possible for a noise reduction of 14.0 dB compared to the original circuit.

Other Circuit Details

It is important to emphasize that the above analysis assumes all Johnson noise generators except for the op-amp itself. In real circuits, inexpensive resistors typically generate noise levels far in excess of the Johnson limit. The usual rule-of-thumb is to use metal film resistors for every component where noise performance is critical. This is easy and not too expensive for through-hole circuit boards, but such resistors are hard to find in small surface mount packages.

Furthermore, the effects of the protection diodes and analog switches on the noise performance have been ignored even though they could be important.

Finally, the high-pass filtering in the above circuits will attenuate the signal strength of lower frequency and out-of-band signals from the PZT. However, some of the noise generators in the circuit are not attenuated and are actually preferentially amplified at lower frequencies. It is recommended that another high-pass filter stage be placed before or after or in conjunction with the summing circuit.

The Effect of Summation on Noise

The summing of the 8 separate signal channel has an interesting effect on the noise performance of the directional receiver. For simplicity, let's suppose that all 8 channels are identical and have the same preamplification gain as the above example prior to summing. This is an interesting case because the modem will be programmed for optional omni-directional reception which functions in precisely this manner.

Naïvely, one might assume that summing 8 channels generates 8 times the signal strength and 8 times the noise level with no effect on the noise performance. However, that is incorrect. The correct noise result for 8 uncorrelated noise sources is,

$$e_{T,sum} = \sqrt{\sum_{j=1}^{8} e_{T,j}^2} \ . \tag{8}$$

So the effect on SNR is $n^{\frac{1}{2}}/n$ or $n^{-\frac{1}{2}}$ where n is the number of channels. So in the omni-directional case the SNR is improved by 9 dB by summation.

However, in the case of directional receiving mode, 4 of the signals have strong signal strength and 4 are greatly attenuated prior to summation. Thus the effect on SNR is only a 6 dB improvement.

Noise Conclusions

For the original circuit we have an equivalent input noise voltage density of 20.4 nV/Hz$^{\frac{1}{2}}$ for a single high gain channel. Assuming that the modem receiver is operating in omni-directional mode the effective total equivalent input noise voltage density after summation is 7.2 nV/Hz$^{\frac{1}{2}}$. If reception is programmed for directional operation, then the effective total equivalent input noise voltage density after summation is 10.2 nV/Hz$^{\frac{1}{2}}$.

While these summed noise results are much better than the single channel numbers, it is useful to note that the summed noise results could be as low as 3.6 nV/Hz$^{\frac{1}{2}}$ if the best circuit were to be used (excluding discrete JFET amplification). Note also, that if the 8 PZT signals were to be conditioned and summed with noiseless amplifiers and circuitry, the effective total equivalent input noise voltage density would be 0.44 nV/Hz$^{\frac{1}{2}}$ for directional operation.

Equivalent Noise Pressure

To compare electronic noise to ocean noise levels it is necessary to divide the noise voltage density values by the sensitivity of the receiver. This converts the noise voltage density to a noise pressure density which can then be directly compared to ocean noise levels. Below are some data analysis and a plot comparing the results to some characteristic ocean noise values.

49

_____

Data analysis: The summing preamp Hofler and Barone built has a gain of 2 for the 190V signal and lower gains for the other channels. (This a simple fixed gain summing preamp that mimics the configuration of the original receiving modem circuit board for directional operation.) The sum of the gains is 2*(2 + 1.58 + 0.526 + 0.116) = 8.44 = 18.53 dB.

The first two columns below are data measured with the first trimode transducer calibrated in the NPS water tank. The measured on-beam-axis RVS for directional trimode operation with the summing preamp was,

Freq.	Meas.(dB)	RVS(dB re 1V/uPa)	Equiv. Noise P (dB re 1uPa/Hz^{½})
15k	+0.5	-189.7	29.9
16k	-1.7	-191.9	32.1
18k	-5.8	-196.0	36.2
20k	-9.5	-199.7	39.9
22k	-12.0	-202.2	42.4
24k	-16.0	-206.2	46.4

Table 4.   Data reduction for directional trimode RVS measurements

Correction factor for RVS → -211.7 dB + 40 dB − 18.53 dB = −190.2 dB. Assumed e_T = 10.2 nV/Hz^{½} for summed directional signals.

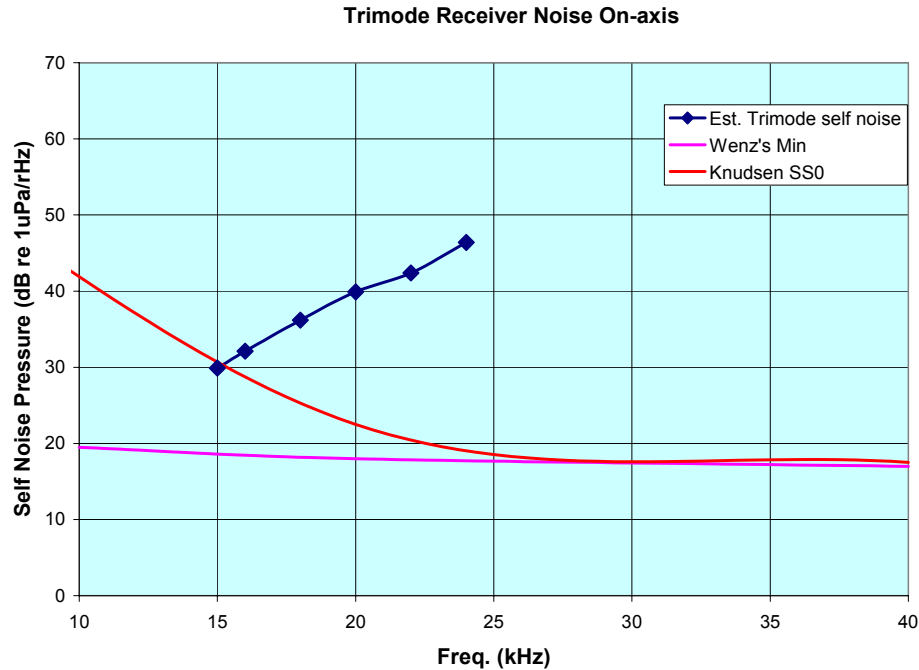**Trimode Receiver Noise On-axis**

Fig. 3. **Estimated Trimode receiver self-noise utilizing theoretical noise voltages based on the original circuit, and measured directional RVS sensitivities. RVS was measured with an NPS summing amplifier in the NPS water tank, with an ITC-1032 projector and a B&K 8103 reference hydrophone.**

Noise with Tuning Inductors

Receiving mode RVS sensitivity data was taken at NPS with the Hofler and Barone Preamp that had been modified with tuning inductors of the value 5.7 mH ±1% connected to each of the 8 channels. (Connected in parallel, I think.)

The raw data are shown below, uncorrected for absolute sensitivity units. Subtract 190.2 dB from the data in the figure to obtain sensitivity in dB re 1V/μPa.
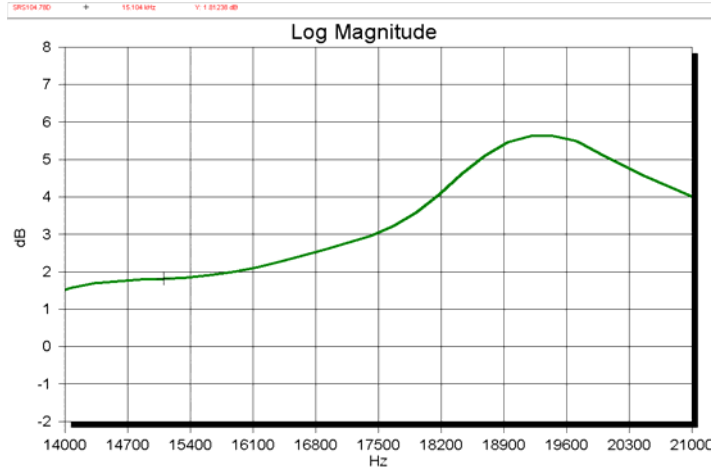

Fig. 4. Raw RVS data with tuning inductors.

These results indicate a much improved sensitivity situation, but before we can begin calculating noise performance, we must recalculate the equivalent input noise voltage values. These values may be slightly worse than before because now the effective susceptance of the PZT with the inductors included is quite large. Before the noise voltage $e_{sa} \ll e_{sp}$, but now they will be more nearly equal.

If we pick the frequency 17.5 kHz as before the new effective PZT reactance is $B_{sp} = j\omega C_{sp} + 1/j\omega L = j(1.264 - 1.596)$ mS = –0.333 mS. Using the exact expression in Eq. (2) we obtain an attenuation factor of 1/4.5 and a value for $e_{sa} = 3.2$ nV/Hz$^{1/2}$.

Zcap = 2.93k + 910, Zcap+RIL = 10.71k. The attenuation cause by R_{HP} is 0.824 or –1.69 dB.

Noise V density	Value (nV/Hz$^{1/2}$)
e_{sp}	14.7
e_{IL}	12.7
e_{HP}	28.4
e_n	8.0
e_{fx}	9.5
e_{sa}	3.2
e_{saIL}	13.1
e_{inp}	11.9
e_T	17.2

Table 5.   Equivalent noise voltage spectral densities for Fig. 1 a).

Thus the corrected (for the R_{HP} attenuator) e_T is 20.9 nV/Hz$^{1/2}$.   If we further correct for the summation improvement we get eT(summed) = 10.4 nV/Hz$^{1/2}$. Note that these noise numbers will now vary substantially over the frequency range of 15 to 30 kHz, unlike before.
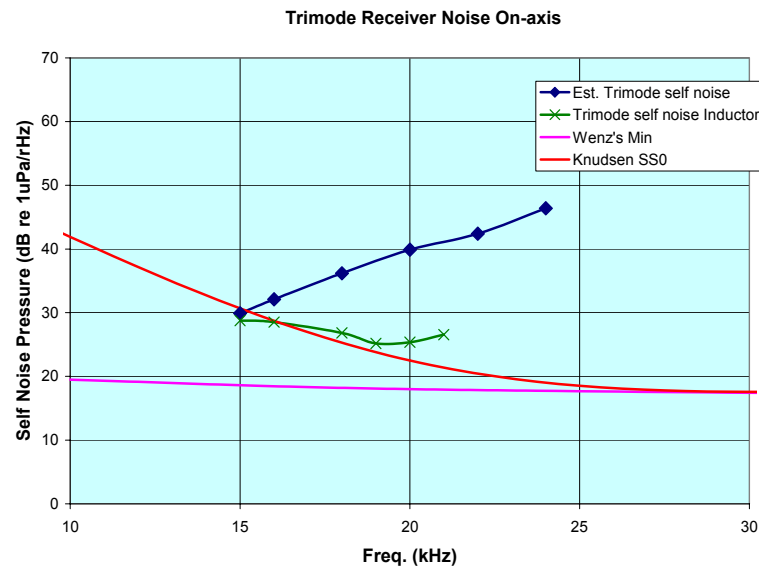

Fig. 5. Equivalent pressure self-noise estimates with tuning inductors included.

LIST OF REFERENCES

Butler, A. L., Butler, J. L., Dalton, W. L. & Rice, J. A. (2000). Multimode Directional Telesonar Transducer, *Proceedings of the IEEE Oceans 2000 Conference*, pp. 1289-1292.

Butler, A. L., Butler, J. L. (2003), *Directional Underwater Acoustic Communications Transducer* (Contract N00014-00-C-0186 CDRL A002 Option I Final Report), Cohaset, MA: Image Acoustics.

Brüel & Kjær. (2002). *Product Data Sheet for Hydrophones 8103, 8104, 8105 and 8106*. Retrieved June 30, 2002, from http://www.bk.dk.

Clark, V. (2002). Sea Power 21: Projecting Decisive Joint Capabilities, *United States Naval Institute Proceedings, 128*(10), 32-47.

Hansen, J. T. (2002). Link Budget Analysis for Undersea Acoustic Signaling (Master thesis, Naval Postgraduate School, 2002).

Hartfield, G. (2003). Performance of an Undersea Acoustic Network during Fleet Battle Experiment (Master's Thesis, Naval Postgraduate School, 2003).

Hofler, T. J. (2003). Modem Receiver Noise Analysis (Report, Naval Postgraduate School, 2003).

International Transducer Corporation. (2003). *ITC-1032 S/N 1097 Data Sheet*. Santa Barbara, CA: International Transducer Corporation.

Love, A. E. H. (1944). *A Treatise on the Mathematical Theory of Elasticity*. New York, NY: Dover Publications.

Rice, J. A. (2000). Telesonar Signaling and Seaweb Underwater Wireless Networks, *Proceedings of NATO Symposium on New Information Processing Techniques for Military Systems*. Istanbul, Turkey.

Rice, J. A. (2003a). *Telesonar Technology for Naval Special Warfare* (FY03 Year-End Report to ONR 321OE). Monterey, CA: Naval Postgraduate School. San Diego, CA: Space & Naval Warfare Systems Center.

Rice, J. A. (2003b). *Telesonar Technology for Off-Board and Deployable Systems* (FY03 Year-End Report to ONR 321SS). Monterey, CA: Naval Postgraduate School. San Diego, CA: Space & Naval Warfare Systems Center.

Rice, J. A., Butler, J. L. & Butler, A. L. (2003). *Compact, Wideband Steered, Directional Telesonar Modem Transducer for Deployable Undersea Sensors* (Presentation at the NDIA Undersea Warfare Technology Conference, March 17 to 20, 2003). Monterey, CA: Naval Postgraduate School.

INITIAL DISTRIBUTION LIST

1. Defense Technical Information Center
    Ft. Belvoir, Virginia

2. Dudley Knox Library
    Naval Postgraduate School
    Monterey, California

3. Jack Butler
    Image Acoustics, Inc.
    Cohasset, Massachusetts

4. Alex Butler
    Image Acoustics, Inc.
    Cohasset, Massachusetts

5. John Baker
    Acoustikos, Inc.
    Cataumet, Massachusetts

6. Vincent McDonald
    SPAWAR Systems Center
    San Diego, California

7. Jim McEachern
    Office of Naval Research
    Arlington, Virginia